2012

Effect of Slip on Flow Past Superhydrophobic Cylinders

Pranesh Muralidhar
University of Massachusetts Amherst, pmuralid@engin.umass.edu

EFFECT OF SLIP ON FLOW PAST SUPERHYDROPHOBIC CYLINDERS

A thesis Presented

by

PRANESH MURALIDHAR

Submitted to the Graduate School of the
University of Massachusetts Amherst in partial fulfillment
of the requirements for the degree of

MASTER OF SCIENCE IN MECHANICAL ENGINEERING

September 2012
MECHANICAL ENGINEERING

EFFECT OF SLIP ON FLOW PAST SUPERHYDROPHOBIC CYLINDERS

A thesis Presented

by

PRANESH MURALIDHAR

Approved as to style and content by:

_____

Jonathan P. Rothstein, Chairperson

_____

Mathew Lackner, Member

_____

Yahya Modarres Sadeghi, Member

_____

Donald L. Fisher
Professor and Department Head

DEDICATION

Dedicated to all the painstaking research on slip and the drag reduction thereof.

ACKNOWLEDGEMENTS

I would like to express my thank you to my advisor, Prof Jonathan Rothstein, for his guidance and support during the course of my Masters study at the University of Massachusetts Amherst. I would like to thank Prof Yahya Modarres Sadeghi and Prof Mathew Lackner for agreeing to serve on the thesis committee and providing valuable feedback and suggestions.

I would like to thank all my lab mates for making the lab a fun place to work. I would also like to thank Nangelie Ferrer for her help in performing some of the experiments. I would also like to thank the professors who made the courses I took a learning experience.

ABSTRACT

EFFECT OF SLIP ON FLOW PAST SUPERHYDROPHOBIC CYLINDERS

09-01-2012

PRANESH MURALIDHAR, B.S., NATIONAL INSTITUTE OF TECHNOLOGY, INDIA

M.S.M.E., UNIVERSITY OF MASSACHUSETTS AMHERST

Directed by: Professor Jonathan Rothstein

Superhydrophobic surfaces are a class of surfaces that have a microscale roughness imposed on an already hydrophobic surface, akin to a lotus leaf. These surfaces have been shown to produce significant drag reduction for both laminar and turbulent flows of water through large and small-scale channels. The goal of this thesis was to explore how these surfaces alter the vortex shedding dynamics of a cylindrical body when coated on its surface, thus leading to an alteration in drag and lift on these surfaces. A cylindrical body was chosen as it is a very nice representative bluff body and sets the stage for predicting the behavior of hydrofoils and other bluff bodies under flow with a slip boundary condition. In this work, a series of experiments were performed which investigated the effect of superhydrophobic-induced slip on the flow past a circular cylinder. In these experiments, circular cylinders were coated with a series of superhydrophobic surfaces fabricated from PDMS with well-defined micron-sized patterns of surface roughness or random slip surfaces fabricated by sanding Teflon cylinders or spray painting superhydrophobic paint on a smooth cylinder. The presence of the superhydrophobic surface was found to have a significant effect on the vortex

shedding dynamics in the wake of the circular cylinder. When compared to a smooth, no-slip cylinder, cylinders coated with superhydrophobic surfaces were found to delay the onset of vortex shedding and increase the length of the recirculation region in the wake of the cylinder. For superhydrophobic surfaces with ridges aligned in the flow direction the separation point was found to move further upstream towards the front stagnation point of the cylinder and the vortex shedding frequency was found to increase. For superhydrophobic surfaces with ridges running normal to the flow direction, the separation point and shedding frequency trends were reversed. The vortices shed from these surfaces were found to be weaker and less interlaced leading to reduced circulation and lift forces on these cylinders. The effect of slip on bluff bodies and separating flow was dealt with in detail in this thesis and the results could be used to predict the impact of these surfaces on the flow past hydrofoils which combine skin friction dominated flow with separating flow.

TABLE OF CONTENTS

Page

LIST OF TABLES

Table Page

LIST OF FIGURES

Figure Page

CHAPTER 1

INTRODUCTION

1.1 Introduction

The flow past a circular cylinder is a benchmark problem in fluid dynamics which has been studied for well over a hundred years with seminal works coming from Strouhal (Strouhal, 1878), Benard (Benard, 1908) and von Karman (Von Karman, 1911) amongst others (Williamson, 1996). As a representative bluff body, studies of flow over a circular cylinder have proven to be instrumental in gaining a fundamental understanding of a broad class of flows where flow separation and vortex shedding occur. At high Reynolds numbers, the onset of vortex shedding is accompanied by a number of unwanted and potentially damaging consequences including increased drag, root mean square lift force and structural vibrations. As a result, there have been a number of studies which have focused on developing both active and passive strategies for reducing the intensity of these vortex-induced vibrations. In this study, we will use superhydrophobic surfaces to investigate the role that slip and the associated reduction in skin-friction drag plays on the flow past circular cylinders. This thesis document is broadly divided into 4 sections. The first chapter (current chapter) makes for background reading on the topic and past work done on the subject. Chapter 2 concentrates on the experimental set up and techniques involved in flow measurements in the current work. Chapter 3 presents and analyzes the results obtained and the thesis is concluded in Chapter 4.

1.2 Past Work: Superhyrdophobic surfaces

Superhydrophobic surfaces were originally inspired by the unique water repellent properties of the lotus leaf (Barthlott & Neinhuis, 1997) and the leaves of a number of other plants (Bhushan & Jung, 2006). It is the combination of a very large contact angle and a low contact angle hysteresis that defines a surface as superhydrophobic. The difference between a hydrophobic surface and a superhydrophobic surface lies not in the surface chemistry, but in its micro or nanoscale surface roughness. Lotus leaves, for example, have micron-sized protrusions covered in waxy crystals while man-made superhydrophobic surfaces are often fabricated using lithographic techniques with precise patterns of micron or nanometer sized ridges or posts (Bico, Marzolin, & Quere, 1999) (Oner & McCarthy, 2000) (Rothstein, 2010) (Zhang, Shi, Niu, Jiang, & Wang, 2008) . In the Wenzel state (Wenzel, 1936), water penetrates into the corrugations on the surface. In the Cassie state (Cassie & Baxter, 1944), the hydrophobicity of the small-scale surface roughness prevents the water from moving into the space between the peaks on the surface resulting in an air-water interface supported between the peaks in the surface roughness. This can be seen schematically in Figure 1 and physically in Figure 2b where the interface is visible through a water drop. It is only in the Cassie state that a surface is truly superhydrophobic and it is in the Cassie state that these surfaces have recently been shown to produce significant drag reduction in both laminar and turbulent flows (Rothstein, 2010).

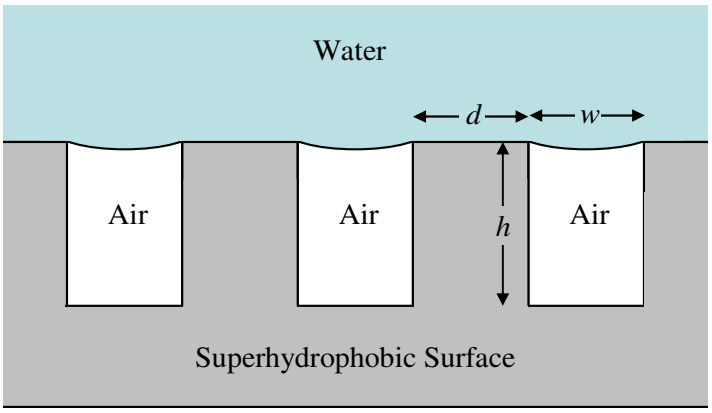

Figure 1: Schematic diagram of a superhydrophobic surface in the Cassie state

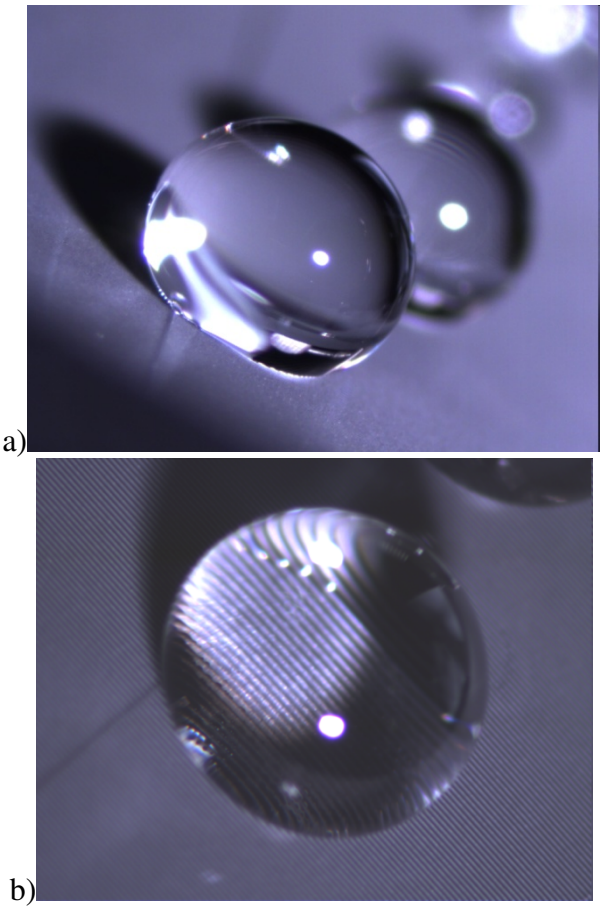

Figure 2: Water drops on a superhydrophobic surface consisting of 30μm wide ridges spaced 30μm apart seen from the side (a) and the top (b)

In flows over superhydrophobic surfaces, the boundary condition experienced by the fluid in contact with the solid is no-slip; however, the air-water interfaces supported between the surface features is essentially shear-free. Ou and Rothstein (Ou & Rothstein, 2005) (Ou, Perot, & Rothstein, 2004) were among the first to experimentally demonstrate that superhydrophobic surfaces could reduce drag in laminar channel flows. Using a series of surfaces with precisely controlled surface topology consisting of regular arrays of micron-sized posts and ridges, they observed drag reductions up to 40%, slip velocities along the superhydrophobic surface of as much as 60% of the free stream velocity and slip lengths up to b = 25μm. Here the slip length is defined using Navier's slip model (Navier, 1823) where the slip velocity, u_0, is proportional to the shear rate experienced by the fluid at the wall, $u_0 = b(\partial u / \partial y)_{y=0}$. The slip length "b" can hence be defined as the additional width you would need to give a channel lined with superhydrophobic surfaces in order to get the same pressure drop. The concept is clearly shown in Figure 3 (Rothstein, 2010), in which the additional length needed for the velocity to become zero is the slip length. Drag reduction and slip length have been found to increase with increasing percentage of shear free air-water interface, increasing spacing between microfeatures and decreasing channel height (Choi, Ulmanella, U., J., Ho, & Kim, 2006) (Choi & Kim, 2006) (Joseph, et al., 2006) (Lauga & Stone, 2003) (Ou, Perot, & Rothstein, 2004) (Ou & Rothstein, 2005) (Rothstein, 2010) (Truesdell, Mammoli, Vorobieff, van Swol, & Brinker, 2006) (Ybert, Barentin, Cottin-Bizonne, Joseph, & Bocquet, 2007) with slip lengths as large as b = 400μm possible for superhydrophobic surfaces with 98% air-water interface (Lee & Kim, 2009).

Superhydrophobic surfaces have also been shown to reduce drag in turbulent channel flows. In turbulent flows, a thin laminar sublayer exists very near to the wall (Pope, 2003). A theoretical analysis by Fukagata *et al*. (Fukagata, 2006) demonstrated how a small alteration of the laminar sublayer can affect the entire turbulent boundary layer and subsequently alter the drag. This effect is demonstrated in the direct numerical simulation (DNS) studies of Min and Kim (Min & Kim, 2004) who performed turbulent channel flow simulations with an arbitrary, but not unreasonable, slip length boundary imposed both parallel and perpendicular to the flow direction. Their simulations demonstrated a decrease in wall shear stress with increasing slip length applied parallel to the flow direction, but an increase in wall shear stress for slip applied perpendicular to the flow direction. More recently, Martell, Perot and Rothstein (Martell, Perot, & Rothstein, 2009) (Martell, Rothstein, & Perot, 2010) used DNS to study the turbulent channel flows over superhydrophobic surfaces containing periodic arrays of micropost and microridge geometries. As in the laminar case, these simulations showed a slip velocity and drag reduction that increase with both increasing microfeature spacing and surface coverage of the shear-free air-water interface. However, unlike in laminar flows, in

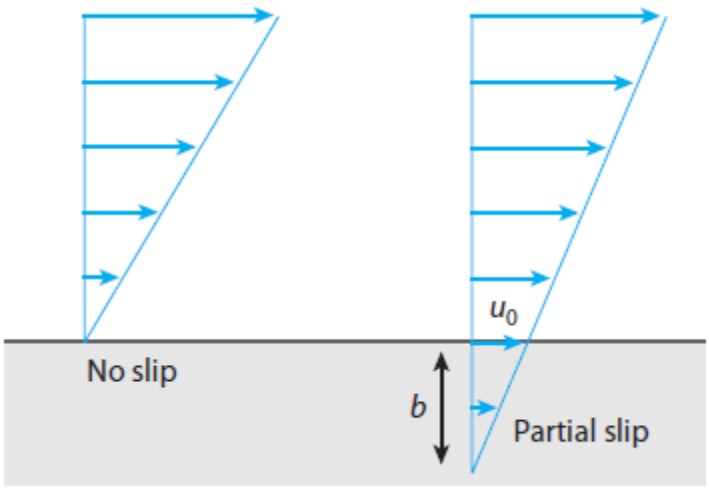

Figure 3: Slip length on a partial slip surface

turbulent channel flows increasing the flow rate and Reynolds number results in an increase in the superhydrophobic drag reduction (Martell, Rothstein, & Perot, 2010).

There are also a few experimental studies of superhydrophobic drag reduction in the turbulent regime (Balasubramanian, Miller, & Rediniotis, 2004) (Daniello, Waterhouse, & Rothstein, 2009) (Gogte, et al., 2005) (Henoch, et al., 2006) (Watanabe, Udagawa, & Udagawa, 1999). Daniello et al. (Daniello, Waterhouse, & Rothstein, 2009) used a rectangular flow cell with smooth and superhydrophobic PDMS walls and studied flows from the laminar regime through transition and into the fully turbulent regime. They observed no drag reduction in the laminar regime because the channel height was much larger than the superhydrophobic feature size. However, in the turbulent regime drag reductions of up to 50% were observed with large slip velocities at the superhydrophobic surface and slip lengths as large as b = 100μm. Drag reduction was found to increase with increasing Reynolds number before reaching an asymptote. These experimental and computational results suggest that in order for turbulent drag reduction

to occur, the spacing between microfeatures must be on the same order as the thickness of the viscous sublayer (Daniello, Waterhouse, & Rothstein, 2009) (Martell, Rothstein, & Perot, 2010).

In addition to these turbulent channel flow experiments, there are three studies that investigated the flow past three-dimensional bodies coated with unstructured superhydrophobic surfaces at moderate to high Reynolds numbers. *Gogte et al.* (Gogte, et al., 2005) observed drag reduction in turbulent flow over a hydrofoil coated with a superhydrophobic surface consisting of hydrophobically-modified sandpaper. Drag reductions of up to 18%, based on combined skin friction and form drag, were reported for the hydrofoil. The overall drag reduction on the hydrofoil decreased with increasing Reynolds number. However only the total drag was reported and the individual contribution of friction and form drag were not deconvoluted. Similar results were observed by Balasubramanian *et al*. (Balasubramanian, Miller, & Rediniotis, 2004) for flow over an ellipsoidal model coated with an unstructured superhydrophobic surface. In both studies, the superhydrophobic surfaces were unstructured so the effect of systematic changes in feature size, spacing and solid fraction could not be studied. In addition, neither of these studies investigated the effect of slip on boundary layer separation which is the primary focus of this paper. More recently, McHale *et al*. (McHale, Shirtcliffe, Evans, & Newton, 2009) used a similar surface to demonstrate up to 30% drag reduction on a superhydrophobic sphere.

Two recent studies have numerically investigated the effect of slip on flow past circular cylinders. You and Moin (You & Moin, 2007) used a combination of both direct numerical simulations (DNS) and large eddy simulations (LES) to investigate the flow

past a circular cylinder containing alternating circumferential bands of partial slip and no-slip. Legendre et al. (Legendre, Lauga, & Magnaudet, 2009) used DNS to investigate circular cylinders with a partial slip boundary condition applied uniformly to the surface of the cylinder (no bands). A detailed summary of the above mentioned work on slip cylinders is made in a following section.

Although no experimental investigations into the effects of slip on circular cylinders have been performed to date, there have been a number of attempts to reduce drag and vibrations on circular cylinders by modifying the surface roughness and texture. Many studies have focused on adding surface protrusions with different shapes and patterns (Zdravkovich, 1981). Lim and Lee (Lim & Lee, 2002) investigated the flow past circular cylinders with a series of U and V-shaped grooves. Although the V-shaped groves had little effect, the U-shaped grooves proved to be quite effective. They produced a 20% drag reduction at large Reynolds numbers ($Re > 5x10^4$), a similar increase in the shedding frequency of the vortices and a significant elongation of the vortex formation region in the wake of the cylinder. These surfaces are similar in many respects to superhydrophobic surfaces, except that they are much larger in scale (mm vs. μm) and fully wetted by the fluid. Thus for these textured surfaces, unlike superhydrophobic surfaces, the effect of the flow is not the result of slip, but the result of the suppression of spanwise vortices in the wake of the cylinder (Lim & Lee, 2002).

1.3 Past Work-bluff bodies and slip

There have been a handful of authors who have concerned themselves with evaluating the flow past bluff bodies coated with a slipping surface. You and Moin (You & Moin, 2007) evaluated the effect of a hydrophobic surface coated on a bluff body

computationally. Bluff bodies can be used in microfluidic devices to enhance mixing and also augment heat transfer. But they tend to suffer from unfavorable effects such as drag and lift induced vibrations. Hence the aim of the study was to see how hydrophobic surfaces could mitigate these effects and for this purpose a circular cylinder was chosen as a representative bluff body. The computational domain (Figure 4) has a cylinder with the entire surface no slip (L_z no slip), entire surface with slip (L_z slip) or with alternate bands of thickness l with slip. The band thickness is varied to be a multiple of the diameter of the cylinder. The slip length considered in this study is of the order of $0.02D$. The work revealed that the case with slip on the entire length of the cylinder was the most effective in reducing drag and rms lift. Slip also proved most effective in the shear layer transition regime of Re=3900 rather than at lower Reynolds numbers. The separation points were found to be pushed downstream, however the Strouhal number was mostly unaffected. The Strouhal Number is the non dimensional frequency of vortex shedding: $\frac{fD}{U}$

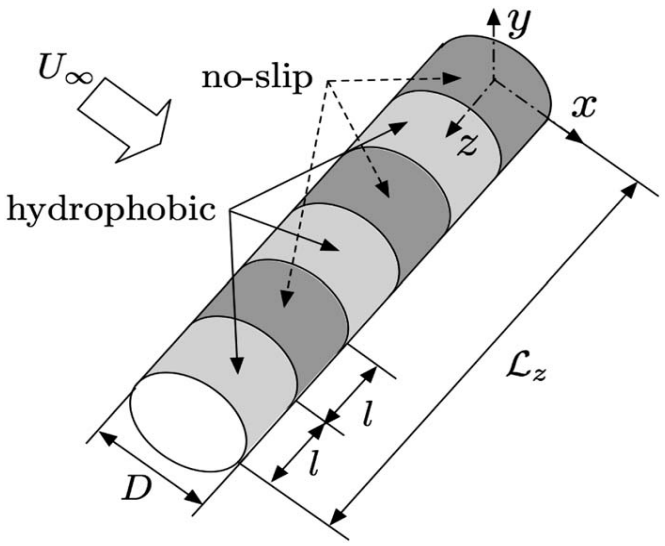

Figure 4: Problem set-up of You and Moin

Legendre et al. (Legendre, Lauga, & Magnaudet, 2009) investigated a generic slip boundary condition on the surface of a cylinder computationally. The ratio of slip length to the radius of the cylinder was termed as the Knudsen number (*Kn*) and varied to study its effect on the wake dynamics. For a given Reynolds Number, an increase in Kn led to a reduction in vorticity and wake size. It was seen that the effect of slip is more pronounced as the Reynolds Number and hence inertial effects scale up. It was also seen that the vorticity shed in the wake decreased as slip increased and this translated directly to a reduction in lift force on the cylinder. An interesting result from this work was that the Strouhal number appeared to increase for the slip cylinders. This was attributed to the increased advection of vorticity on the surface of the cylinder with increase in slip which would lead to an increase in the frequency of shedding. The slip investigated in this study did not have any particular orientation, rather it was an arbitrary slip length imposed on the surface.

Gogte et al. (Gogte, et al., 2005) investigated the effect of textured superhydrophobic surfaces on drag reduction past hydrofoils and for droplets moving down an inclined plane. The part of their work related to the current work is the hydrofoil experiments. It was found that a textured superhydrophobic surface outperforms an untextured coated smooth surface which outperforms the rough surface with no coating on it. The authors also clearly established that drag reduction decreases with an increase in Reynolds number. A similar decrease in drag reduction with increase in Reynolds number was reported by Balasubramanian *et al*. (Balasubramanian, Miller, & Rediniotis, 2004) for flow over an ellipsoidal model coated with an unstructured superhydrophobic surface.

1.4 Past Work-lift force on cylinders

A lot of work has been done on understanding the lift force on cylinders. The force on both stationary and vibrating cylinders has been looked at. However lift force data on stationary cylinders between Re=190 and Re=6000 is relatively hard to come by due to the weak force in this regime and the difficulty associated with measuring the force using transducers. Apart from a lot of work already done on the topic, the spread in the value of the RMS lift coefficient is quite huge with a lot of discrepancy between the values measured by different methods. Furthermore, the lift force on a vibrating cylinder is much more than those of a stationary cylinder since the mass of the cylinder, the damping of the springs and the added mass of water all contribute to the force. Hence it is much easier to measure unsteady lift forces on a vibrating cylinder (VIV case) rather than a stationary one. Drescher, 1956 (Drescher, 1956) was among the first to measure the fluctuating lift force on cylinders. He measured the sectional wall pressure distribution around the cylinder at a Re=100000 and derived the lift force out of it. Blackburn and Melbourne, 1996 (Blackburn & Melbourne, 1996), investigated the effect of free stream turbulence on the lift force on cylinders in the regime Re=100000 to Re=500000. Semiconductor strain gages in full bridge configuration were employed to measure the lift forces and they found that an increase in free stream turbulence increased the force on cylinders in the supercritical regime. Further data on the lift force on cylinders in the sub-critical regime have been provided through numerical simulation data from Beaudan and Moin (Beaudan & Moin, 1994), Kravchenko et al. (Kravchenko & Moin, 1998) and a few others. West and Apelt (West & Apelt, 1993) investigated the forces on a cylinder in the range of Reynolds numbers from 10^4 to $2.5*10^5$ and provided conclusive data on the

same. The study aimed at addressing some of the uncertainties in the data presented on the topic over the past years and also to study spanwise effects on the lift force and pressure distribution on cylinders. The experiments covered the upper subcritical regime of Reynolds Number, while our experiments concentrate on the lower subcritical regime. Norberg, 2003 (Norberg, 2003) gave a comprehensive review of lift measurements on stationary cylinders over the past few decades, comprising both experimental and numerical studies. The Reynolds number range covered in this work was from Re=47 to Re=$2*10^5$. The author also looked at the various ways used by people in the past to measure the lift on cylinders. The methods covered here include force methods, which sense the lift force on a vibrating element mounted with a strain gage or piezoelectric transducer, pressure methods, which use the sectional pressure distribution on the cylinder to arrive at the lift force and momentum methods, which use the velocity data in the wake of the cylinder to calculate the lift force. Norberg has also compiled the 2-D and 3-D lift RMS lift coefficients from various authors and plotted it on a master curve versus 6 decades of Reynolds Number. The plot clearly shows the variability of the lift coefficients obtained by different methods and by different authors over the years. Of particular interest is the momentum method for measuring lift, where only high resolution velocity data is required in the wake of the cylinder to measure the force. No knowledge of the pressure field is required. This method is ideal for scenarios where the lift force is too small to be measured using transducers.

Momentum techniques typically involve estimating the time rate of change of vorticity in the wake of the cylinder and calculating the unsteady fluid dynamic forces on the cylinder using the impulse concept, first explained by Lamb (Lamb, 1945). The

impulse concept states that the lift force on the cylinder is equal and opposite to the force which the cylinder exerts on the flow to produce the oscillating flow patterns. Lighthill (Lighthill, 1986) showed that Lamb's impulse concept could be used to calculate force acting on the cylinder in a 3-D flow as the time rate of change of the moment of vorticity around the cylinder. The force is given as:

$$F = \frac{\mathrm{d}}{\mathrm{d}t}\left(\frac{1}{2}\rho\int \boldsymbol{x} \wedge \boldsymbol{\omega}\,\mathrm{d}V\right). \tag{1.1}$$

Here, the factor of ½ in the equation stems from a $\frac{1}{N-1}$ prefactor where N is the dimension of the space under consideration (Noca, 1997). For a 2-D flow, the lift force reduces to (Lin & Rockwell, 1996):

$$L = \rho\frac{\mathrm{d}}{\mathrm{d}t}\int_{\mathrm{A}} x\omega_z \mathrm{d}A. \tag{1.2}$$

ω_z is the vorticity in the z-plane, dA is composed of piecewise area elements of the 2-D control volume chosen from the PIV data.

Recently, a number of groups have been using these non-intrusive techniques to measure lift because, as described above, the oscillating lift force from the cylinder is often below the transducer resolution. Lin and Rockwell (Lin & Rockwell, 1996) used the time variation of spatial vorticity packets in the wake of the cylinder to estimate the fluid dynamic forces acting on an oscillating cylinder in otherwise quiescent water. In their study the cylinder was started up from rest and only a few cycles were observed so as to confine all of the vorticity to the region in the wake of the cylinder they could interrogate with PIV. This was done because the impulse method requires the time evolution of all the shed vortices to give an accurate force estimation value. This could only be achieved if the domain is large enough that the vortices decay before they reach

the edge or, for the case of a start-up flow, if the vorticity is confined within a finite domain. Lin and Rockwell (Lin & Rockwell, 1996) found good agreement of the lift coefficient estimated by the impulse method with the measured value over the course of 1.5 shedding cycles. This work was aimed at a proof-of-concept validation of the impulse method for estimating lift force. Later, Noca et al. (Noca, 1997) (Noca, Shiels, & Jeon, 1997) set out to compute the lift force acting on a cylinder using vorticity data from an arbitrary, finite control volume surrounding the body. Noca (Noca, 1997) showed that the impulse method could be extended to finite control volumes if the flux of vorticity out of the control volume is taken into account. Noca's modified version of the impulse equation is shown:

$$-F_{ext} = -\frac{1}{N-1}\frac{\mathrm{d}}{\mathrm{d}t}\int \boldsymbol{x} \wedge \boldsymbol{\omega}\, \mathrm{d}V + \oint_S \hat{\boldsymbol{n}}.\boldsymbol{\tau}_i\, \mathrm{d}S. \tag{1.3}$$

where the tensor $\boldsymbol{\tau}_i$ is:

$$\boldsymbol{\tau}_i = \frac{1}{2}u^2\boldsymbol{I} - \boldsymbol{uu} - \frac{1}{N-1}\boldsymbol{u}(\boldsymbol{x} \wedge \boldsymbol{\omega}) + \frac{1}{N-1}\boldsymbol{\omega}(\boldsymbol{x} \wedge \boldsymbol{u}). \tag{1.4}$$

Noca et al. (Noca, Shiels, & Jeon, 1997) tested their approach by performing 2-D PIV at the midspan of the cylinder to capture velocity fields over several shedding cycles. The cylinder was also coupled to a force balance and the spanwise averaged lift force was directly measured. They found that the 2-D lift value measured from the vorticity lift formulation over-predicted the transducer-measured lift force by an order of magnitude. Along the span of the cylinder, vortices shed at different phases and hence the force measured by a transducer (which is a spanwise averaged measurement) is significantly lesser than that which would be obtained from a 2-D sectional measurement. Moreover, they looked at the self consistency of the results than at absolute values of lift coefficients

and this 2-D measurement satisfied that adequately. This method proves ideal for the scenarios where the lift force is too small to be measured using conventional strain gauges and force transducers. Although this 2-D method does not provide a realistic estimate of the lift coefficient, it might prove quite effective when doing a one-one comparison of the sectional lift force from two cylinders.

1.5 Summary

In summary, there has been a lot of work dealing with characterizing the shedding dynamics and forces on cylinders placed in a flow. Recently, there has also been a good amount of work in developing superhydrophobic surfaces and utilizing them for drag reduction in channel flows. However there have been no experimental studies so far on the effect of slip in the flow past bluff bodies. This thesis seeks to provide a definitive answer to this question by combining the phenomenon of slip with the concept of flow separation and looking at the outcomes of the same.

CHAPTER 2

EXPERIMENTAL SET UP

A water tunnel (Engineering Laboratory Design, Model 501) with a 15.2x15.2x45.7cm test section was used for making both qualitative and quantitative measurements of flow past a circular cylinder with a velocity up to approximately U = 1m/s, which corresponds to a Reynolds numbers of approximately $Re = UD/\nu \leq 10,000$. Here U is the average centerline velocity upstream of the cylinder measured with a Pitot tube, D is the diameter of the cylinder and v is the kinematic viscosity of the water. A schematic diagram of the flow cell is shown in Figure 5. The diameter of the circular cylinders were D = 12.7mm resulting in an aspect ratio of $W/D=H/D$ = 12.

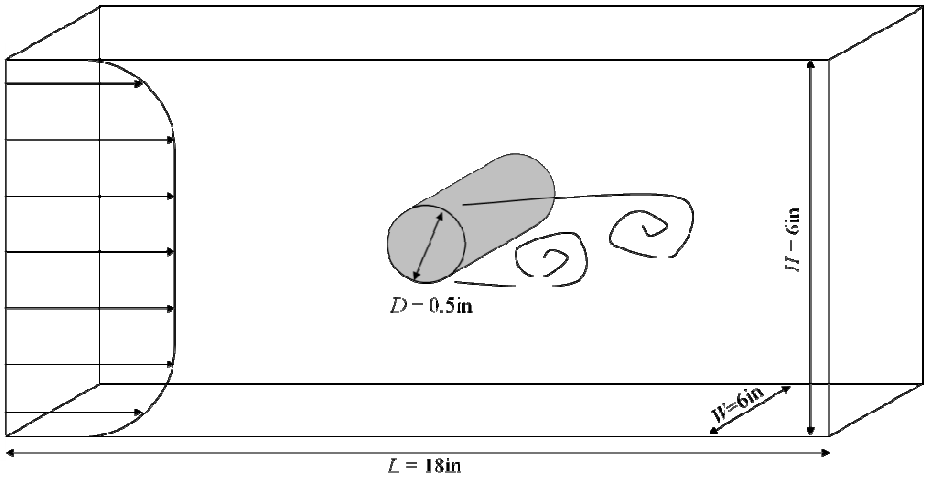

Figure 5: Schematic diagram of flow cell used in the experiments

2.1 Directional Superhydrophobic surface fabrication

Soft-lithography techniques were used to produce a series of precisely patterned superhydrophobic surfaces in polydimethylsiloxane (PDMS) (Daniello, Waterhouse, & Rothstein, 2009) (Xia & Whitesides, 1998). This lithographic technique is quite useful

and flexible for producing patterns on the micron or even the nanometer lengthscales. The soft lithography process starts by using a CAD package to design the size, spacing and alignment of the desired micro-patterned surface. For these experiments, superhydrophobic surfaces were designed with two different sets of ridges. The first surface contained d = 15μm wide ridges spaced w = 15μm apart and the second contained d = 30μm wide ridges spaced w = 30μm apart. In addition to testing the effect of size and spacing of the superhydrophobic ridges, the effect of alignment of the ridges, both aligned and normal to the flow direction, was investigated. Once the design was complete, the CAD file was printed on a high-resolution transparency at 5080 dots per inch. The transparency served as a mask for contact photolithography using a positive photoresist (SU-8) on a silicon wafer (MacDonald & Muller, 1997). The photoresist was exposed through the mask and developed, leaving behind a positive image of the mask in photoresist. At this point, the cross-linked photoresist remaining on the silicon could itself be used as the master to create a negative of its pattern in PDMS. This was done by first spin coating the PDMS onto the silicon wafer and curing the PDMS in an oven. The replica was then peeled from the master creating a micropatterned surface on a flexible elastomer substrate. It is naturally hydrophobic without further chemical reaction and it can be applied to almost any substrate or scaffold, flat or curved, while maintaining the ordered and precise patterning that makes the use of silicon wafers and lithographic techniques so desirable.

2.2 Surface coating protocol

Because PDMS is a flexible rubber, it makes it possible to mold onto complex three-dimensional geometries. However, the single degree of curvature of the circular

cylinder makes it ideal for coating because it eliminates the need for complicated cutting, folding and seaming of the superhydrophobic surfaces. A threaded cylinder was taken and was coated with PDMS, which filled up the threads of the rod. This was baked for 30 minutes in an oven at 60^{o}C to harden the coating. The superhydrophobic patch was then cut to the exact size required and one extreme of the patch was stuck along the length of the cylinder by applying pressure and curing it in the oven for 30 minutes at 60^{o}C. Now that one edge of the patch was cured on to the cylinder, the latter was rolled so that the patch enveloped the cylinder and the other edge of the patch actually met the cured edge along a single thin line, which then became the seam. It was then wrapped carefully in aluminum foil and allowed to cure overnight. A single seam did exist running axially along the length of the cylinder, after curing. Special care was taken to minimize the height of the seam which was kept below approximately 50μm along its entire length. The seam was placed at the rear stagnation point of the cylinder, $\theta = 180°$. The impact of the seam was studied by comparing the separation and shedding frequency for both a smooth aluminum cylinder and smooth PDMS coated cylinder containing a seam. No discernible difference between these two cylinders could be measured suggesting that the presence of the small seam does not have a large impact on the flow when placed along the trailing edge of the cylinder.

2.3 Particle Image Velocimetry

The wake structure of the cylinders was quantified using PIV (Particle Image Velocimetry). Illumination was provided using a continuous wave Argon Ion laser with a maximum power of 400mW. A cylindrical lens was used to split the beam into a laser sheet of thickness of 500μm. The flow was seeded with 50μm diameter neutrally-buoyant

silvered glass spheres (Sphericel, Potters Industries, Carlstadt, NJ). The motion of the particles under the laser light sheet was captured using a high-speed video camera (Phantom V4.2). A commercial particle image velocimetry (PIV) code (DaVis, LaVision Gmbh) was then used to correlate the particle displacements and calculate both velocity vector fields and vorticity fields. Proper orthogonal decomposition (POD) was then used to isolate the primary vortices and determine their shedding frequency and the Strouhal number (Shi, Liu, & Wan, 2010).

2.4 Breaker ridges

There are a number of experimental challenges associated with maintaining a coherent air-water interface. The microfeatures on a superhydrophobic surface are susceptible to damage occurring during installation or operation as well as defects introduced during fabrication. Posts are especially vulnerable which is why the focus of this study is on ridges. If a superhydrophobic surface is operating near the maximum static pressure for which an air-water interface can be maintained and a single post is missing or damaged, the spacing between posts will double locally and the entire superhydrophobic surface can be wetted by water thereby destroying its efficacy. In order to mitigate this problem, a concept called breaker ridges, shown schematically in Figure 6, and developed already in the lab was used. This makes the surface more robust, less prone to catastrophic damage and capable of supporting significantly larger static or dynamic pressures, therefore increasing the range of applications and uses for superhydrophobic drag reduction.

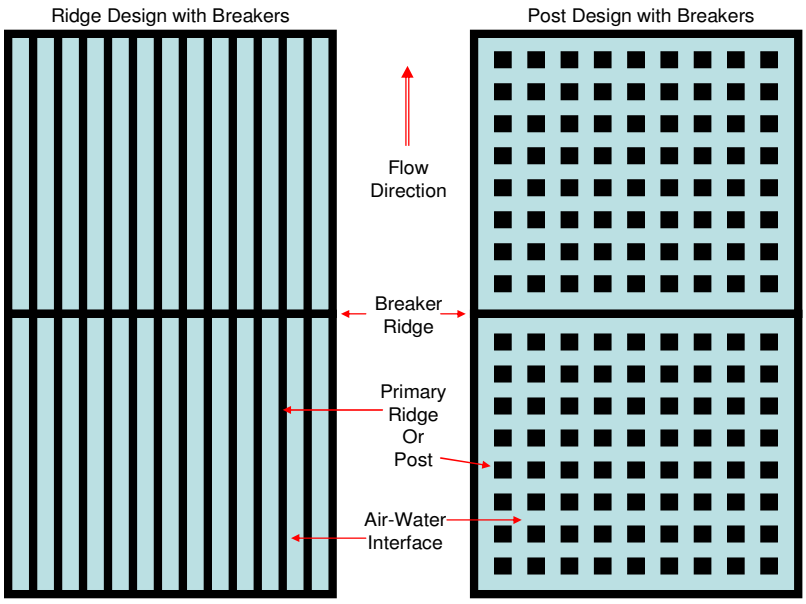

Figure 6: A schematic showing breaker ridges for arrays and posts

There is a large difference for drag reduction if a ridge is aligned in the flow direction or normal to the flow direction. In laminar flow, if the ridges are aligned with the flow, they are twice as effective as ridges aligned normal to the flow direction (Lauga & Stone, 2003). In turbulent flow, ridges aligned normal to the flow direction actually increase drag (Min & Kim, 2004) while ridges aligned in the flow direction can greatly reduce drag up to 50% (Daniello, Waterhouse, & Rothstein, 2009). In the case of a superhydrophobic surface containing ridges, the surface design used in the breaker ridge construction incorporates both ridges in the flow direction and normal to it as seen schematically in Figure 6. The ridges across the flow direction are the breaker ridges. The breaker ridges were added at intervals of 2mm which is roughly two orders of magnitude larger than the spacing between the primary ridges. The relatively low density of breaker ridges means that they should have very little impact of the drag reduction of

the surface, but have a significant impact on the ability of the surface to maintain the air water interface which is critical for the purpose of these surfaces.

2.5 Randomized slip surfaces

So far, the slip described is directional in nature, as in, the slip ridges are either aligned parallel to or transverse to the flow direction. The current work also looks at superhydrophobic cylinders with random isotropic slip on the surface. To achieve this, one way was by sanding Teflon cylinders with 320 grit sandpaper (Nilsson, Daniello, & Rothstein, 2010). Sanding produced random roughness elements (microfeatures) on the already hydrophobic Teflon surface, thereby making it superhydrophobic. Another way was by spray painting a cylinder with a superhydrophobic paint (Cytonix LLC, WX2100^{TM}). This imposed random, isotropic slip on the surface of the cylinder by virtue of the random distribution of the superhydrophobic particles from the paint, on the surface. The shedding and lift force characteristics of these randomized slip surfaces are addressed in this thesis. The majority of work however deals with the ridged slip cases and a detailed characterization of those cases is made.

CHAPTER 3

RESULTS

3.1 Vortex shedding modes

As described by the excellent review of Williamson (Williamson, 1996) amongst others, a number of different flow regimes exist for the flow past a no-slip circular cylinder. The transition to each flow regime has been quantified and the vortex dynamics studied in great detail. Below a Reynolds number of approximately $Re < 5$ the flow does not separate. Between $5 < Re < 49$, the wake behind the cylinder contains two steady, counter-rotating vortices. Beyond a Reynolds number of $Re > 49$, the steady vortices in the wake of the cylinder becomes unstable and a laminar vortex shedding regime persists up to a Reynolds number of about $Re \approx 200$. In this regime, A-mode vortices are shed at a dimensionless shedding frequency known as the Strouhal number, $St = f\,D/U$ which increases with increasing Reynolds numbers. This can be seen in the measurements of Strouhal number for a smooth surface presented in Figure 8 which match the well established trends in the literature (Williamson, 1996). The A-mode is characterized by a spanwise wavelength of the "secondary" vortices that can be several cylinder diameters. These secondary vortices have differences in shape and feature compared to the more large scale and coherent Karman vortices. However, the same mechanism responsible for generation of the Karman vortices is responsible for the secondary vortices. At larger Reynolds numbers, B-mode vortices become the dominant mode and are characterized by spanwise wavelengths of approximately one cylinder in diameter (Brede, Eckelmann, & Rockwell, 1996). As the Reynolds number continues to increase, the flow in the wake of the cylinder becomes increasingly three-dimensional and disordered. Above a Reynolds

number of approximately Re>1000, the shear layer passing around the cylinder becomes unstable, the wake becomes fully turbulent, the separation point moves upstream along the cylinder and the Strouhal number begins to decrease slowly with increasing Reynolds number (Williamson, 1996).

3.2 Onset of shedding

Initially it was decided to find the critical Reynolds Number for onset of shedding so as to see if there was a delay in shedding due to slip. The critical Reynolds numbers for the onset of vortex shedding are presented in Table 1 to within the velocity and Reynolds number resolution of the water tunnel. The lower limit in velocity of the water tunnel corresponded to a Reynolds number of $Re_{\min}$ = 70 and the minimum possible velocity increment corresponded to an increase of 20 in Reynolds number. The precision to which the critical Reynolds number for the onset of vortex shedding could be determined was less than optimal. However, these measurements clearly demonstrate that by coating a cylinder with a superhydrophobic surface and inducing slip along the surface of the circular cylinder the onset of vortex shedding is delayed to larger Reynolds numbers. The largest shift was observed for the 30μm-30μm superhydrophobic surface for which the critical Reynolds number was observed to shift from around Re = 70 for the smooth surface to between 70 and 90. A visual comparison of the 30-30 ridges (flow direction), the sanded Teflon surface and the spray painted superhydrophobic surface with the smooth surface is shown in the streak images of Figure 7. No observable shift in the critical Reynolds number was observed for the surface containing ridges aligned perpendicular to the flow direction. Unfortunately, because of the uncertainty in the exact

value of the critical Reynolds number in the experiments, a direct comparison with the literature is not possible at this point.

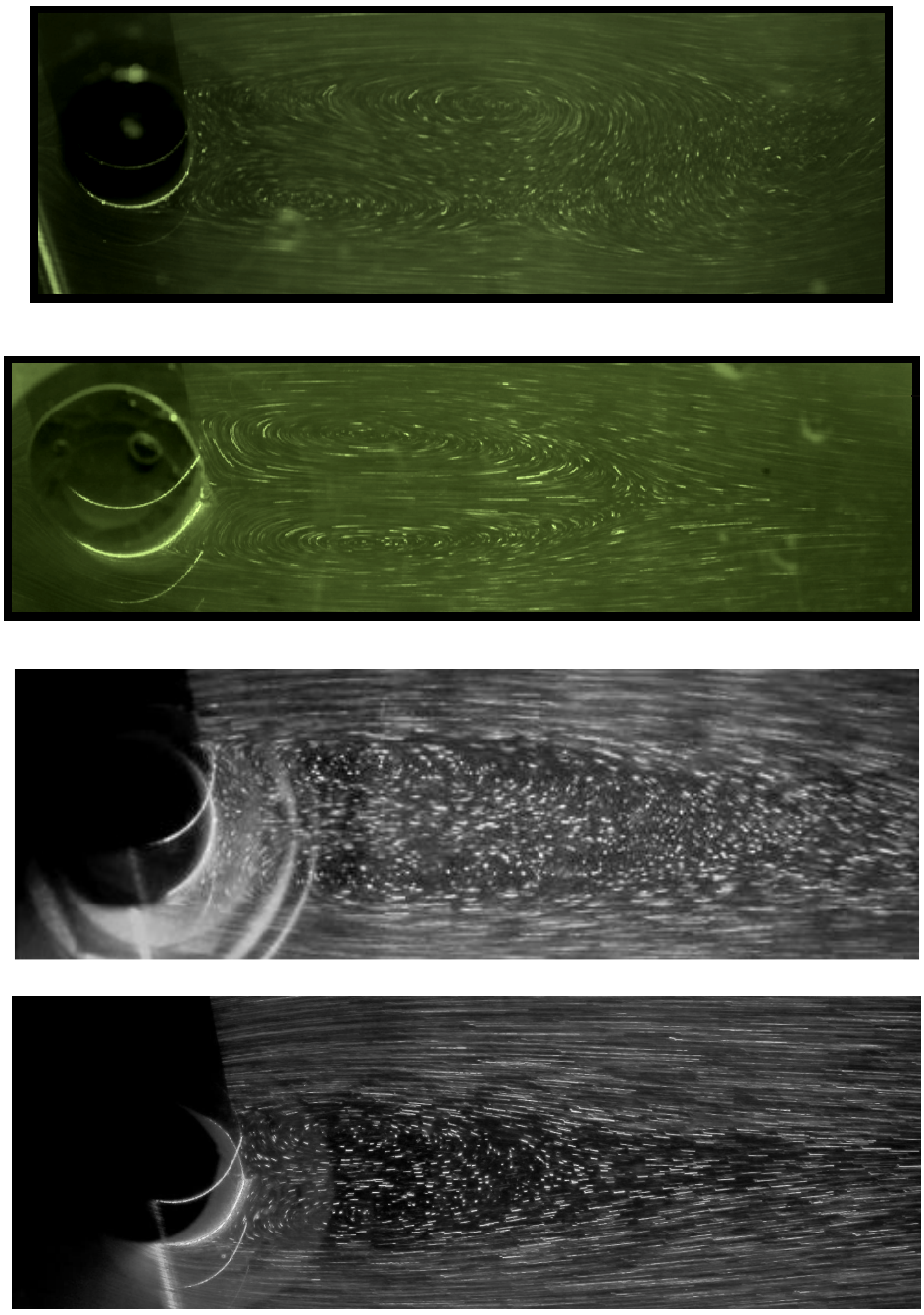

Figure 7: Streak images comparing shedding, from top to bottom, of a no slip surface, a 30-30 superhydrophobic surface with ridges aligned in flow direction, a sanded Teflon surface and a spray painted superhydrophobic surface at Re=70

3.3 Effect of slip on Strouhal Number

The next feature of bluff body flow that was addressed is the dependence of Strouhal Number on slip and its orientation. The Strouhal number is the non dimensional frequency of vortex shedding. Using a combination of PIV (to get the vector fields) and POD (Proper Orthogonal Decomposition- to isolate the primary vortices using a combination of eigen modes), the Strouhal number was calculated. As shown in Figure 8, for the smooth circular cylinder, the Strouhal number followed the expected trends; first increasing rapidly at low Reynolds numbers before reaching a maximum and slowly decreasing with continued increase in Reynolds number. The application of superhydrophobic coatings to the surface of the circular cylinder had a significant effect on the vortex shedding dynamics. This can be seen quite clearly from the Strouhal number trend in Figure 8. Using superhydrophobic surfaces with ridges aligned in the flow direction increased the Strouhal number by as much as 25% from $St = 0.2$ to $St = 0.25$ at a Reynolds number of $Re = 1000$. The increase in Strouhal number was observed starting at a Reynolds number of $Re = 300$ and was maintained for all the Reynolds numbers tested, although the magnitude of the increase in Strouhal number was found to decrease as the Reynolds number increased beyond $Re > 2000$. The reversal of this trend below $Re < 300$ was likely the result of delay in the onset of vortex shedding for this superhydrophobic surface. The overall effect on Strouhal number seemed to be nearly independent of the size and spacing of the micro-ridges, with both the 15μm-15μm and 30μm-30μm ridges showing similar enhancement to the Strouhal number.

Table 1: **Critical Reynolds Numbers for vortex shedding onset**

Surface	Smooth	15μm-15μm Ridges Aligned in Flow Direction	30μm-30μm Ridges Aligned in Flow Direction	15μm-15μm Aligned Normal to Flow Direction	Sanded Teflon (Random slip)	Spray painted cylinder (Random slip)
Re_{crit} for Onset of Vortex Shedding	< 70	70-90	70-90	<70	70-90	70-90

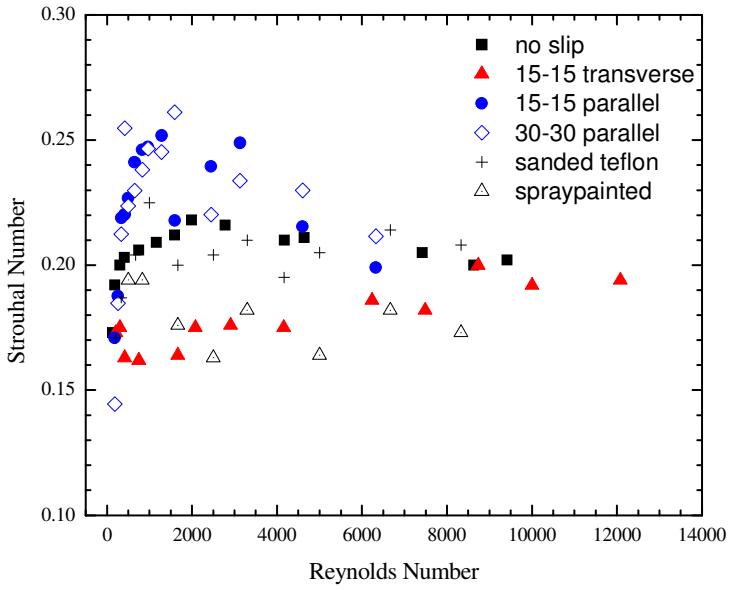

Figure 8: Dimensionless vortex shedding frequency, Strouhal number, as a function of Reynolds number for circular cylinders with a smooth surface (■), superhydrophobic surfaces with ridges aligned in flow direction (w=d=15μm (●) and w=d=30μm (◊)), a superhydrophobic surface with ridges aligned normal to the flow with w=d=15μm (▲), a sanded Teflon surface (□) and a superhydrophobic spray painted exterior (8)

It is clear from Figure 8 that the alignment of the microstructure on the superhydrophobic surface plays a significant role in the vortex dynamics. In laminar flows, aligning the ridges normal to the flow direction reduces the drag reduction by a factor of two (Lauga & Stone, 2003), while in turbulent flows, DNS simulations have shown that transverse ridges significantly reduce the slip velocity on the superhydrophobic surface while essentially eliminating the drag reduction (Martell, Rothstein, & Perot, 2010) or in some instances increasing the drag (Min & Kim, 2004). Additionally, the alignment of the ridges normal to the flow direction enhances the axial

velocity fluctuations along the ridges. As seen in Figure 8, for the superhydrophobic ridges aligned axially along the cylinder and normal to the flow direction, the trend in Strouhal number was quite different. In this case a 25% reduction in the Strouhal number was observed at a Reynolds number of Re =1000 with the effect of the superhydrophobic surface again slowly diminishing as the Reynolds number was increased to Re = 10,000. For the scratched Teflon cylinders, the Strouhal Number was predominantly unchanged from that of the no slip case, as also observed by Daniello et al. in the forced vibration experiments (Daniello, Personal Communication). For the spray painted cylinders however, the Strouhal number was consistently lesser than the smooth cylinder over the range of Reynolds Numbers tested. This might be due to enhanced slip on the spray painted surface as compared to the sanded Teflon surface due to a greater percentage of air coverage over the solid surface.

3.4 Wake characteristics of slip cylinders

The effect of the superhydrophobic surface on the vortex shedding dynamics can be further investigated by comparing streak images from the different cylinders at a fixed Reynolds number. In Figure 9 and Figure 10, streak images for Reynolds numbers of Re = 180 and Re =490 are presented for comparison. The differences in these images are quite striking. First, notice that the formation region of the separated vortex is much larger for the superhydrophobic surfaces. The end of the formation region is defined as the location along the centerline where oscillating wake characteristics are first observed (Lim & Lee, 2002). Increases in the size of the formation region have been shown to directly correlate to a reduction in drag (Lim & Lee, 2002). One consequence of the increased length of the formation region is that the

vortices shed from the superhydrophobic cylinders were significantly elongated/stretched in the flow direction, both before and after the onset of vortex shedding. This was likely caused by the slip velocity along the cylinder and the resulting increased velocity within the boundary layer. A final observation is that the degree of interlacing of the shed vortices downstream of the superhydrophobic cylinders was significantly reduced. In other words, the centers of the vortices shed from the superhydrophobic cylinders were offset further from the centerline than vortices from the smooth cylinder. These observations, which are perhaps more easily observed in the PIV velocity vector fields presented in Figure 11, might also suggest a reduction in the strength of the rms lift force.

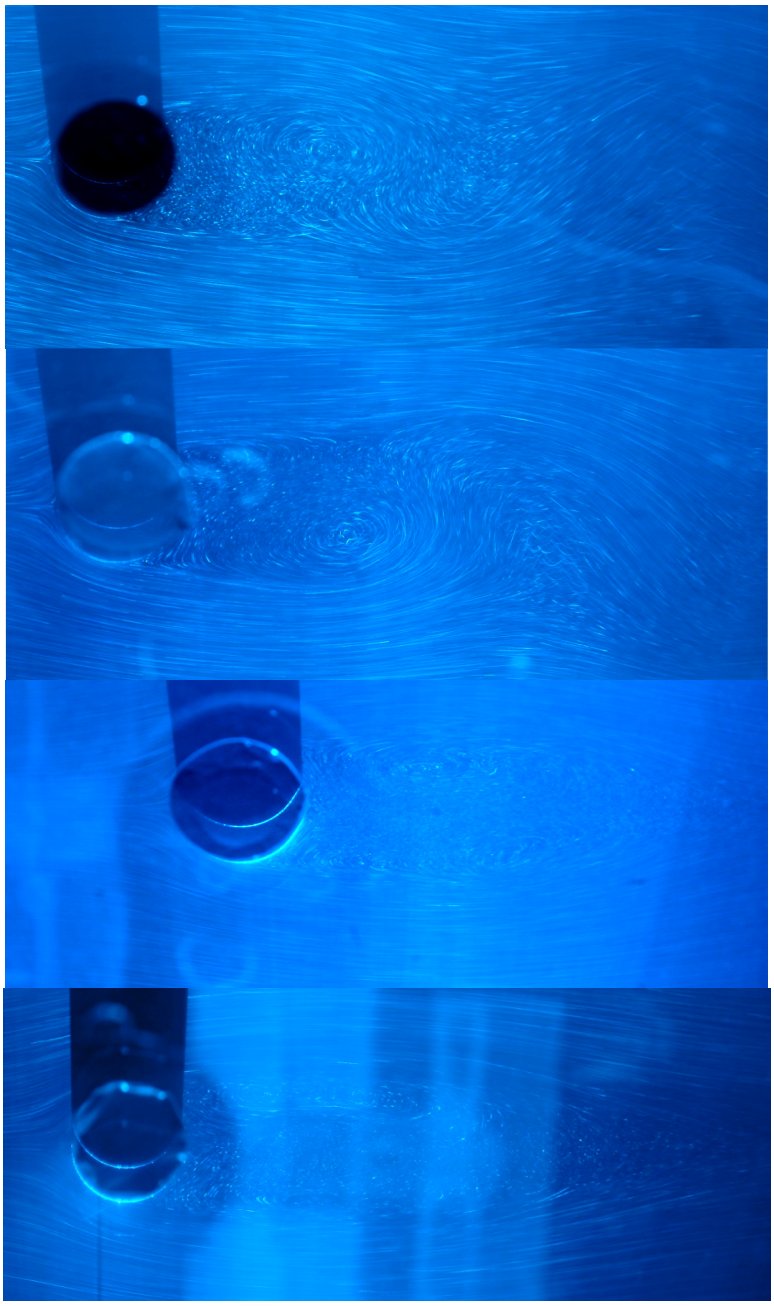

Figure 9: Streak images showing flow separation and vortex shedding past a series of cylinders at a Reynolds number of Re = 180. The images include, from top to bottom, a smooth cylinder, a superhydrophobic cylinder containing 15µm wide ridges spaced 15µm apart and aligned in the flow direction and a superhydrophobic cylinder containing 30µm wide ridges spaced 30µm apart and aligned in the flow direction and a superhydrophobic cylinder containing 15µm wide ridges spaced 15µm apart and aligned perpendicular to the flow direction.

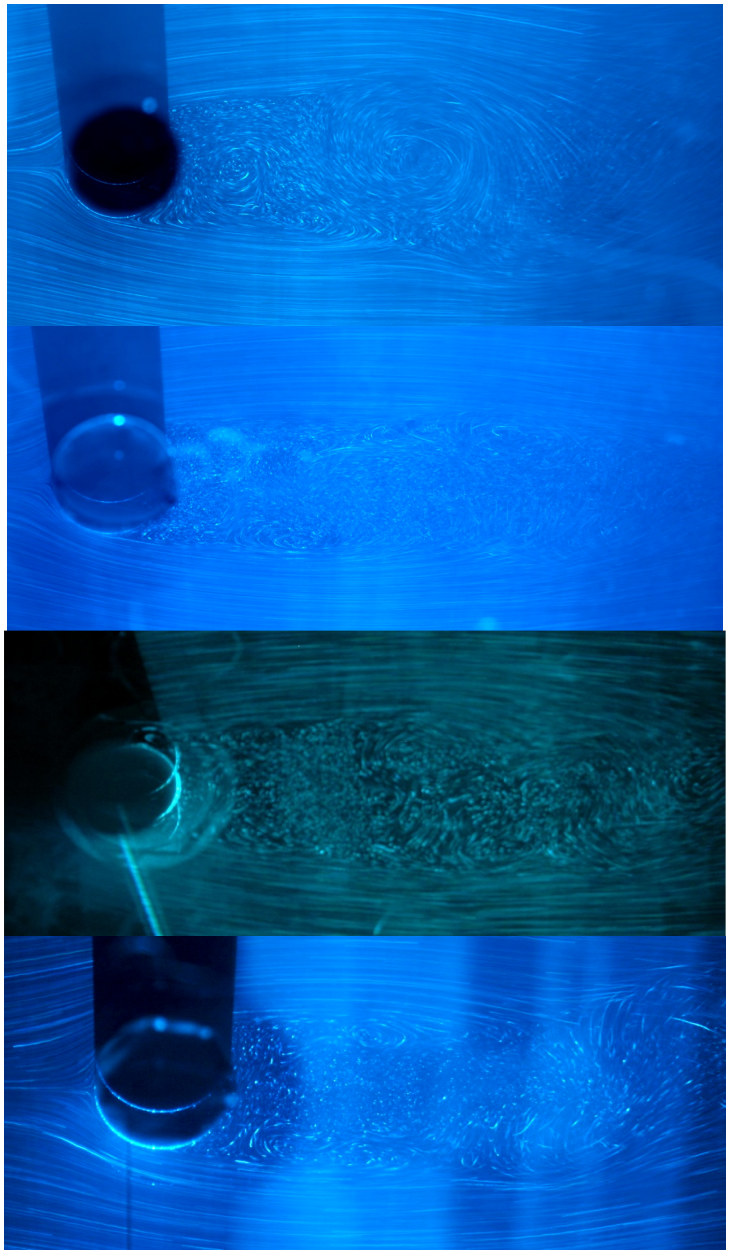

Figure 10: Streak images showing flow separation and vortex shedding past a series of cylinders at a Reynolds number of Re = 493. The images include, from top to bottom, a smooth cylinder, a superhydrophobic cylinder containing 15µm wide ridges spaced 15µm apart and aligned in the flow direction, a superhydrophobic spray painted cylinder, and a superhydrophobic cylinder containing 15µm wide ridges spaced 15µm apart and aligned perpendicular to the flow

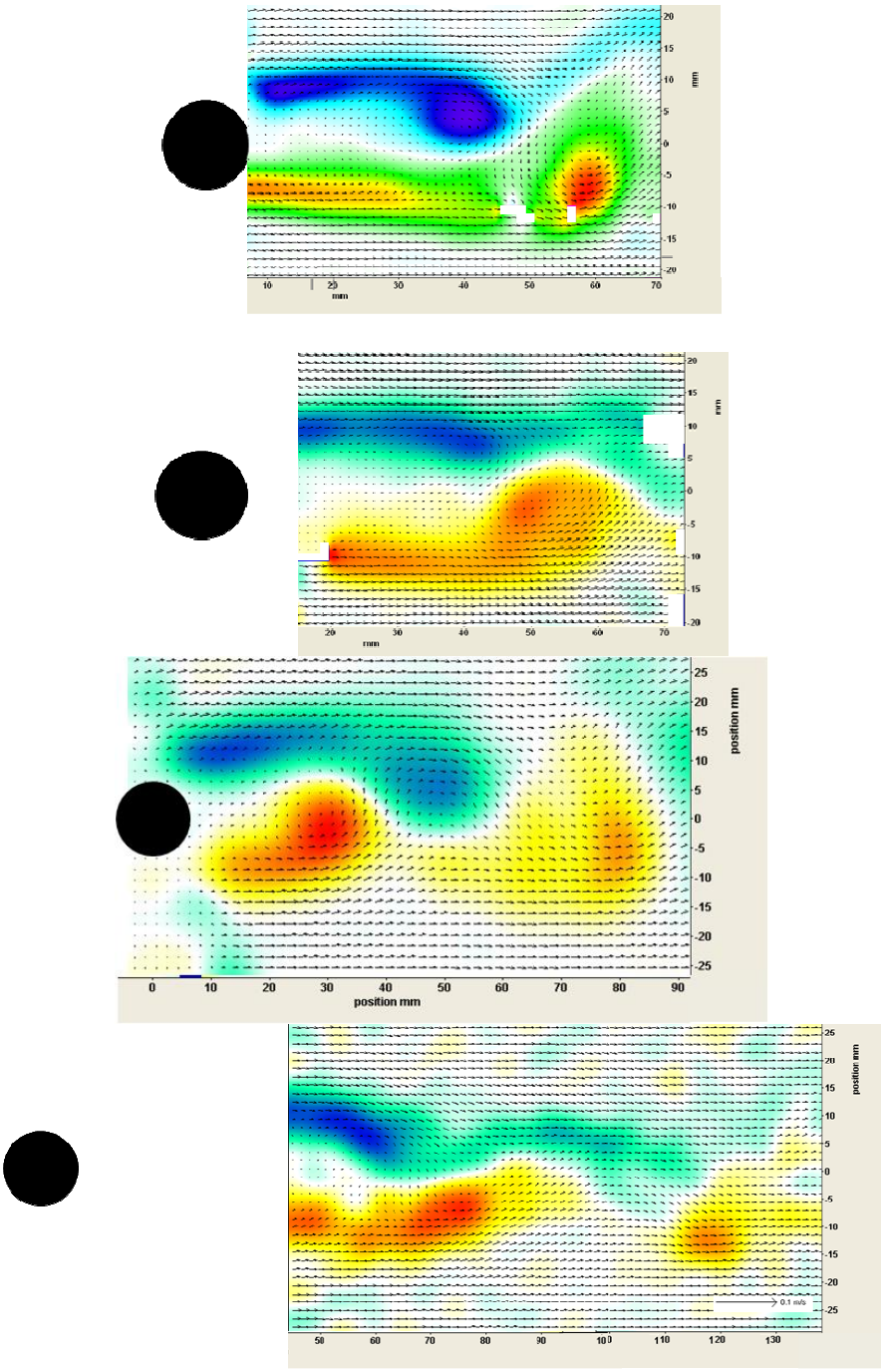

Figure 11: Particle image velocimetry vector fields with vorticity overlaid as a color map. The vector fields were correlated downstream of, from top to bottom, a smooth circular cylinder, a superhydrophobic cylinder containing 15µm wide ridges spaced 15µm apart and aligned perpendicular to the flow direction, a superhydrophobic cylinder containing 15µm wide ridges spaced 15µm apart and aligned in the flow direction, and a superhydrophobic cylinder containing 30µm wide ridges spaced 30µm apart and aligned in the flow direction at Re=256

3.5 Flow separation

A detailed study was done using streak images on the ridged superhydrophobic surfaces to understand the effect of slip on the angle of flow separation from the cylinder. From the streak images in Figure 9 and Figure 10, it is also possible to observe changes in the separation point from the cylinder as a function of superhydrophobic coating. The separation point is quantified in Figure 12 as a function of Reynolds number for the smooth cylinder as well as the three ridged superhydrophobic cylinders. The separation point from the smooth cylinder followed the well-established trends. Near the onset of vortex shedding, the separation angle was approximately $\theta_{sep} = 110°$. Here $\theta_{sep} = 0°$ corresponds to the stagnation point at the leading edge of the cylinder. It should also be noted that all the separation angle measurements were only accurate to within $\pm 1°$. With increasing Reynolds number, the separation point moved very quickly upstream, past the equator and eventually asymptotes around $\theta_{sep} = 85°$. The separation point measured for the superhydrophobic surfaces follow the same general trend; however, for the surfaces with ridges aligned in the flow direction, the separation angle was consistently smaller at all but the smallest Reynolds numbers. This was likely the result of the slip velocity at the surface of the cylinder increasing the velocity and linear momentum of the fluid within the boundary layer or perhaps reducing the base suction. Just the opposite trend was observed for the superhydrophobic surface containing ridges aligned normal to the flow direction; the separation angle retreated more slowly and asymptotes at a slightly large value of than both the smooth and other superhydrophobic surfaces. Another interesting observation is that the 15μm ridges appeared to have a more significant impact on the separation angle than the 30μm ridges. At least at the lower Reynolds numbers,

this was likely the result of the significant delay observed in the onset of vortex shedding. However, at high Reynolds numbers it may be a result of the gradual failure of this surface on the front stagnation point at high Reynolds numbers where the stagnation pressure was enough to drive the air-water interface into the spaces between some of the ridges and transition the superhydrophobic surface from a Cassie to a Wenzel state. With the cylinder underwater, the air-water interface between ridges was highly reflective and appeared to shimmer. The transition from Cassie to Wenzel state coincided with a change in the appearance of the surface from reflective to matte black which is the color of the PDMS. For the superhydrophobic surface with 30μm ridges, above a Reynolds number of Re = 4,000 roughly 10% of the surface around the leading edge of the cylinder was gradually driven into the Wenzel state. The 15μm ridges were found to remain in the Cassie state over all the Reynolds numbers tested.

3.6 Swirling Strength

Due to the slip on the surface of these cylinders, the vorticity elements shed did not have as much rotation as the no-slip case and hence the vortices were weaker in the case of the slip cylinders. Quantifying the strength of the vortices would be very useful in understanding the properties of slip and no-slip bluff body flows. Vorticity, the curl of the velocity vector, identifies both shear flows and vortex cores (Adrian, Christensen, & Liu, 2000) and hence higher vorticity does not essentially mean large scale rotation of fluid element; it could also mean regions of shear. Vorticity is thus a very noisy vortex identification technique and its use for identifying and quantifying vortex strength is limited. Instead, a quantity termed “swirling strength” is widely used to identify vortices in the flow. Swirling strength is defined as the square of the positive imaginary Eigen

value of the local velocity gradient tensor. Stronger vortices have higher swirling strength. From a comparison of the no slip and the ridged slip case, it is seen that the cylinders with ridges of slip shed lesser vorticity in the wake than the smooth case. The procedure used for the analysis was as follows: The time varying velocity fields were averaged for each cylinder to get rid of all the local noise and spurious vectors and arrive at an average velocity field, averaged over a number of shedding cycles. The swirling strength of this field was computed and a threshold was set for the swirling strength as $T = \frac{\omega_{max}}{100}$. Values within this threshold were averaged and an average swirling strength value was computed. The threshold served to get rid of all the spurious noise arising out of portions where there was no light and from places with faulty correlations. A comparison of the average swirling strength magnitude is shown in Figure 13, which shows the variation of swirl strength with Reynolds Number for the smooth cylinder and the cylinders with ridges of slip, both in the flow direction and transverse to the flow direction. The swirling strength of the average velocity field from a slip and a no slip cylinder is shown in Figure 14. The wake consists of two steady counter rotating domains of swirl, on account of the averaging.

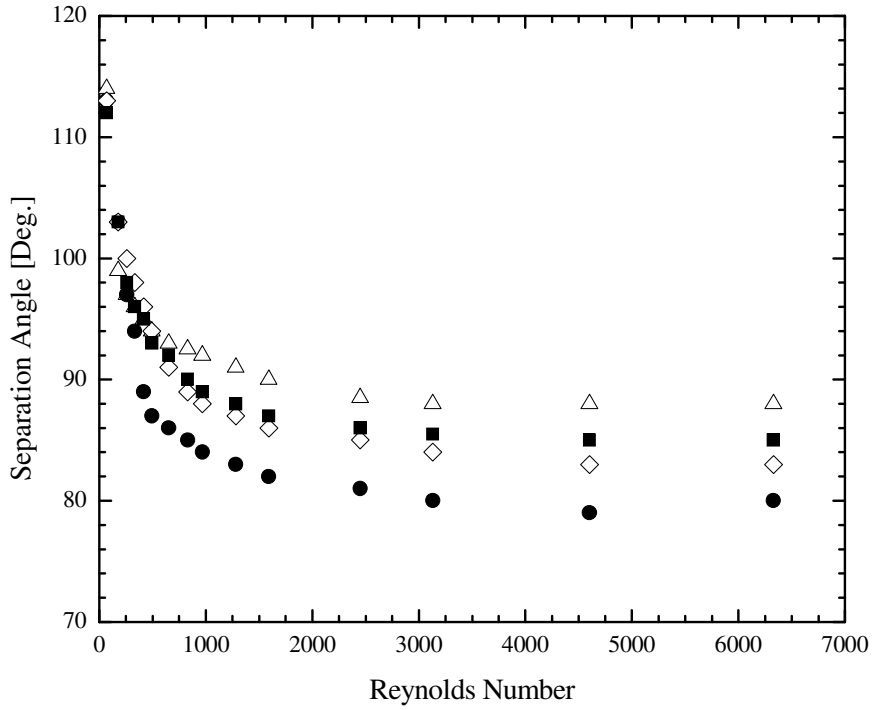

Figure 12: **Separation angle as a function of Reynolds number for a circular cylinders with a smooth surface (■) and superhydrophobic surfaces containing *w*=30μm wide microridge spaced *d*=30μm apart (◊) and *w*=15μm wide microridge spaced *d*=15μm apart aligned in the flow direction (●) as well as *w*=15μm wide microridge spaced *d*=15μm apart aligned normal to the flow direction (Δ). Separation angle is measured from the upstream stagnation point of the cylinder.**

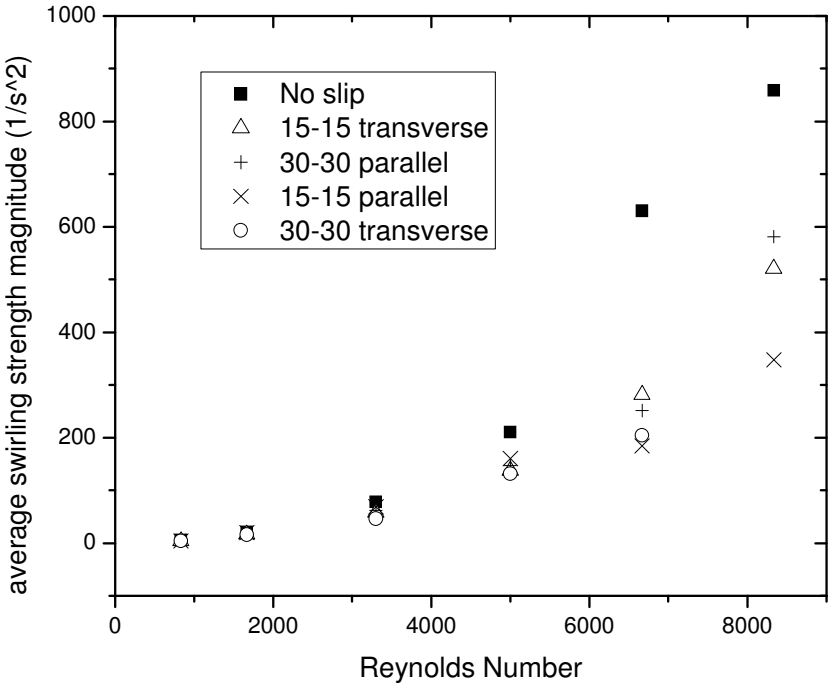

Figure 13: **Average swirling strength in the wake as a function of Reynolds Number. Data include a smooth cylinder (■) and superhydrophobic surfaces containing *w*=30μm wide microridge spaced *d*=30μm apart (□) and *w*=15μm wide microridge spaced *d*=15μm apart aligned in the flow direction (x) as well as *w*=15μm wide microridge spaced *d*=15μm apart (∆) and *w*=30μm wide microridge spaced *d*=30μm apart (*O*) aligned normal to the flow direction.**

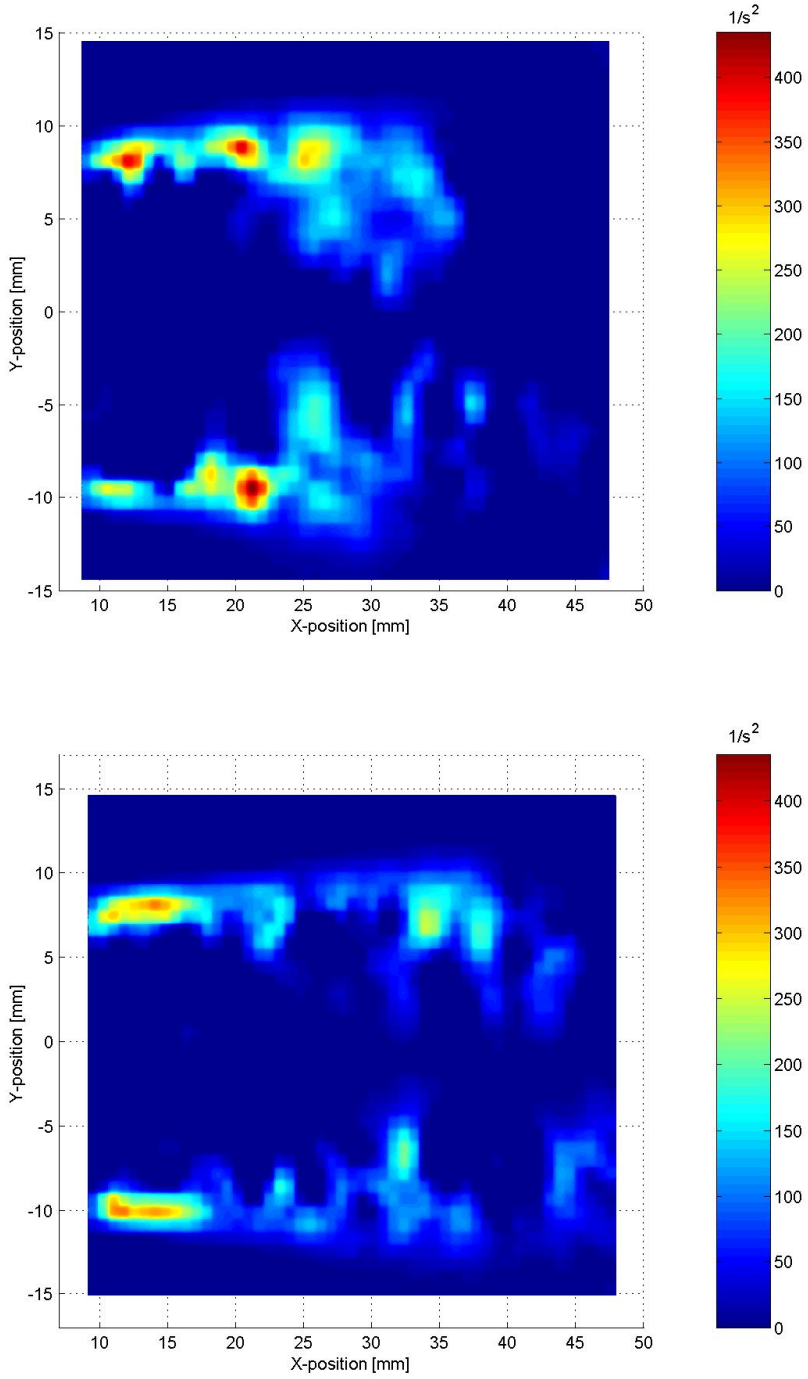

Figure 14: Contours showing swirling strength of the time-averaged wake of a smooth cylinder (top) and a superhydrophobic cylinder with *w*=15*μ*m wide microridge spaced *d*=15*μ*m apart aligned transverse to the flow at Re=3300. The contours are scaled the same way, from 0 to 435 $\frac{1}{s^2}$.

3.7 Turbulent Kinetic Energy

Turbulent Kinetic Energy (TKE) is the mean kinetic energy per unit mass possessed by the eddies in a turbulent flow. The flow in the wake of the cylinder can be divided into a mean and a fluctuating part. TKE can be thought of as the kinetic energy of fluctuating turbulent flow, $0.5(u'^2 + v'^2)$. The TKE was computed from the time varying velocity fields for the smooth and the ridged slip cylinders. Then a threshold of $T = \frac{K_{\max}}{10}$ was applied to the TKE distribution, similar to the approach followed for the swirling strength, and an average TKE was calculated as a function of Reynolds Number. Figure 15 shows a comparison between the TKE of the smooth cylinder and the cylinders with ridges of slip. It is clear that the cylinders with ridges of slip have consistently lower TKE than the smooth case.

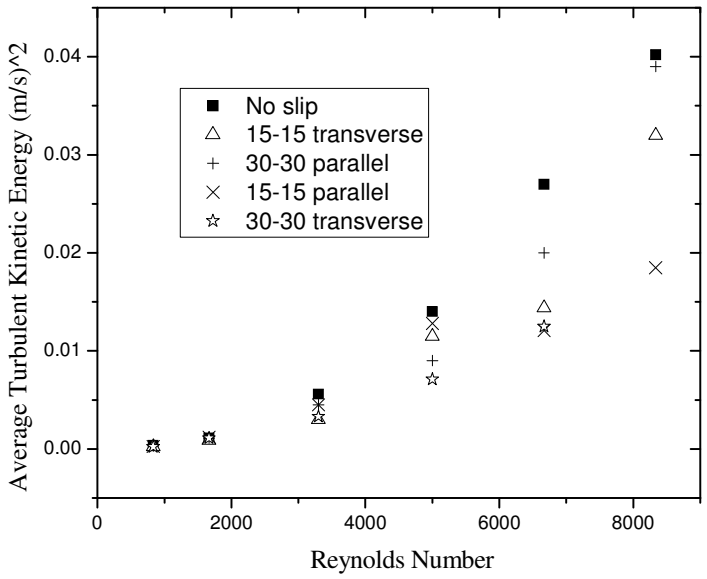

Figure 15: Turbulent Kinetic Energy measurements as a function of Reynolds Number in the wake of no slip and various superhydrophobic cylinders, the details of which are shown in the inset of the graph.

3.8 Drag force measurements

The drag force on the cylinders was measured by rigidly mounting the cylinders to a force transducer. The load indicating element of the transducer was a push-pull strain gage and the cylinder was mounted so that there is an inline force in the principal direction on the strain gage and hence the drag force was directly read off the transducer. To eliminate the differences in drag arising out of differences in wetted length (length of the immersed cylinder) between the smooth and the slip cylinders, the same cylinder was tested in both the Cassie and the Wenzel state and hence both slip and no-slip comparisons were made on the same cylinder. To achieve the Wenzel state of wetting, the cylinder was dunked, when in the Cassie state, into a container of water and was placed in a vacuum chamber for a couple of minutes to drive the air out of the

microfeatures. What ensued was the water going into the features to replace the air sucked out by the vacuum, which resulted in a Wenzel state of wetting. Disappointingly, no differences in drag could be inferred from the data. The drag measurements from the Cassie and the Wenzel state of the ridged slip cases were within a few percent of each other and this was attributed to random error of experimentation and no drag differences were assumed from this. This is in line with what was observed by Legendre et al. (Legendre, Lauga, & Magnaudet, 2009) in the simulations of flow past cylinders with varying degrees of slip on the surface. They found that, in the case of very low Knudsen Numbers (ratio of slip length to radius of cylinder), the effect of slip on the drag is negligible, which is precisely the effect that was seen in the drag measurements. This is due to the very low values of Knudsen Number achievable in the current study. The drag on a cylinder in a flow is composed of 2 components: a "form drag", which arises due to separation of flow and the resulting pressure differential between front and back sides of the cylinder, and a "friction drag", which arises due to skin friction drag acting on the cylinder surface. For a non-streamlined body like a cylinder, the friction drag forms a few percent of the total drag, and form drag dominates. These superhydrophobic surfaces do not affect the separation point so much that a difference in form drag could be seen. Hence, only a difference in friction drag would amount to a total of 1-2 % change in the total drag force which would be well within the limit of the force transducer. It is believed that this was the reason for the drag force being same in the Cassie and Wenzel states. Figure 16 shows the drag curve comparisons for the Cassie and Wenzel states of a cylinder with ridges of slip in the flow direction (30-30) and one with ridges of slip transverse to the flow direction (15-15).

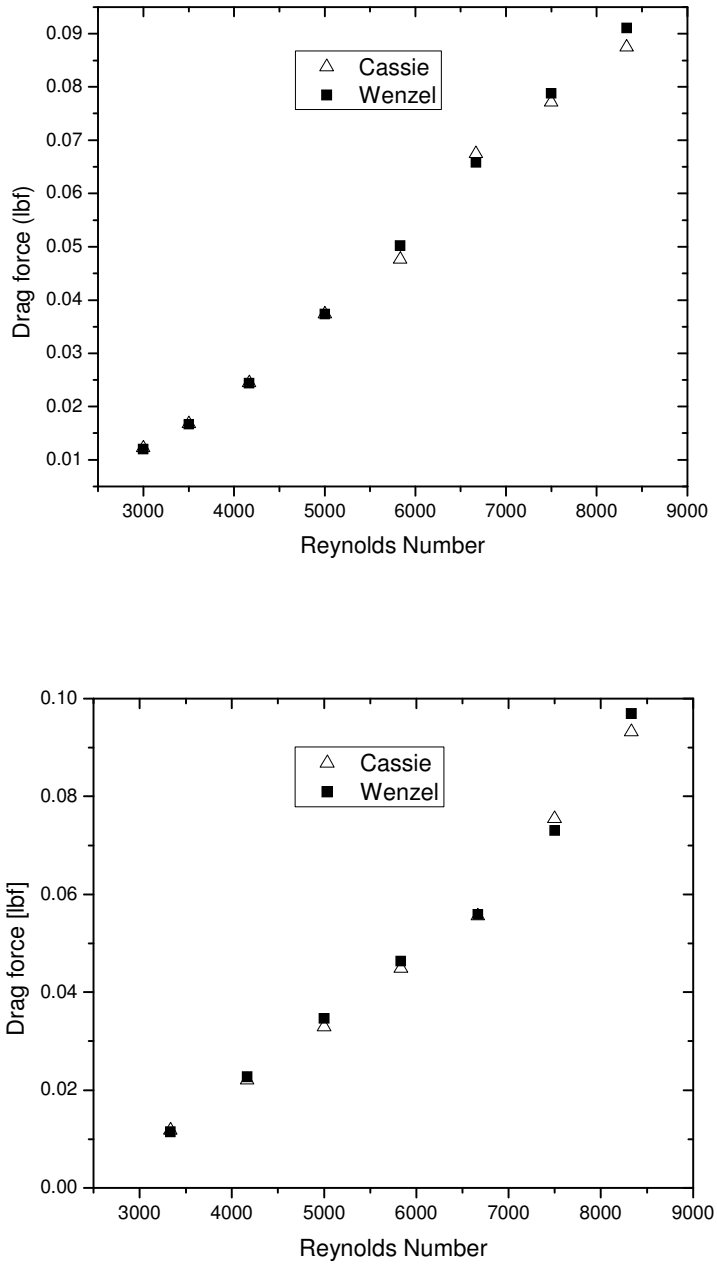

Figure 16: Drag force comparison of cassie and wenzel states of a superhydrophobic cylinder with w=15μm wide microridge spaced d=15μm apart aligned transverse to the flow (top) and a superhydrophobic cylinder with w=30μm wide microridge spaced d=30μm apart aligned parallel to the flow (bottom)

3.9 Lift force measurements

Lift force is the oscillating force acting on a cylinder in the cross-flow direction when it is subjected to a flow. If the cylinder is free to oscillate, these vibrations can build up and be damaging to the structure in question. Indeed, galloping, a form of VIV (Vortex Induced Vibration) from a non-symmetrical structure was responsible for the Tacoma Bridge disaster, the collapse of a huge man made structure. It was decided to see if slip had an effect on the lift force acting on the cylinders under study here. It was already obvious that the vortices shed from the cylinders with slip were weaker and were less correlated. This hinted at the fact that the RMS lift force on the cylinder had to go down with slip.

The lift force on a cylinder in cross flow oscillates with time as vortices are shed with alternating positive and negative vorticity. The mean lift force on the cylinder is zero. As a result, to characterize the strength of the lift force on a cylinder the Root Mean Square (RMS) value of the lift force is often used, $F_{L,RMS}$. A lift coefficient can be defined from the RMS lift force as:

$$C_{L,\,RMS} = \frac{F_{L,\,RMS}}{\frac{1}{2}\rho U^2 DL}. \tag{3.1}$$

Here, ρ is the density of water, U is the free-stream velocity, D is the cylinder diameter and L is the spanwise length of the cylinder exposed to flow. The coefficient obtained using equation 3.1 gives the spanwise averaged RMS lift coefficient in the case of a 3-D measurement. There is a wide spread in the value of the RMS Lift Coefficients in the literature (Norberg, 2003). It extends from 0.1-0.2 for 3-D spanwise averaged lift measurements to O (1) values for 2-D measurements. 3-D measurements are typically

obtained either through direct measurement of lift force using force transducers while 2-D measurements are made using velocimetry measurements that focus on a single plane in the wake of the cylinder and cannot resolve variations in the flow along the length of the cylinder.

In the current experiments, lift force on a stationary cylinder was sought. The diameter of the cylinders used in this study was D=12.7mm. For these small cylinders, lift forces of the O (10^{-2}) N was estimated. Initially, the lift force was attempted to be measured by mounting strain gages in a half bridge configuration around the cylinder. In a half bridge configuration, one strain gage is in compression and the other strain gage is under tensile strain, thereby the signal strength doubles. However, it was found that the lift forces were so weak that the signal was being overridden with noise. Shielding the strain gages did not solve the problem. A new approach was to mechanically amplify the lift force arising from the cylinder. The cylinder was coupled to the load sensitive element of the force transducer through a hinge. The analog signal was directly sampled using Labview at a rate roughly 25 times the Strouhal frequency. An amplification factor of roughly 15:1 was achieved using the hinge. However, at this point, the cylinder was taking the stiffness of the load sensitive element of the force transducer into its system and was starting to act like a cylinder subjected to flow, mounted on "springs", the springs being the stiffness of the load sensitive element. Hence vastly higher lift coefficients were calculated from the set up than would be expected from a stationary cylinder. This approach was also abandoned at this point.

Instead of trying to measure lift forces using conventional techniques, it was decided to switch to a non-intrusive method of measuring lift. Momentum techniques

presented a way of achieving this. The modified impulse method of Noca (Noca, 1997) (Noca, Shiels, & Jeon, 1997) (as described in the Past Work section) was used for the lift formulation. In the present experiments, lift force on a stationary cylinder was sought. The wake of a stationary cylinder extends to a very large distance downstream and hence it was near but impossible to get both a field of view and enough detail to capture all of the vorticity. Hence Noca's (Noca, 1997) technique works well for the purpose since it is used to compute the force on a cylinder with a finite control volume. Equations 1.3 and 1.4 were used for the analysis.

3.9.1 Lift estimation procedure

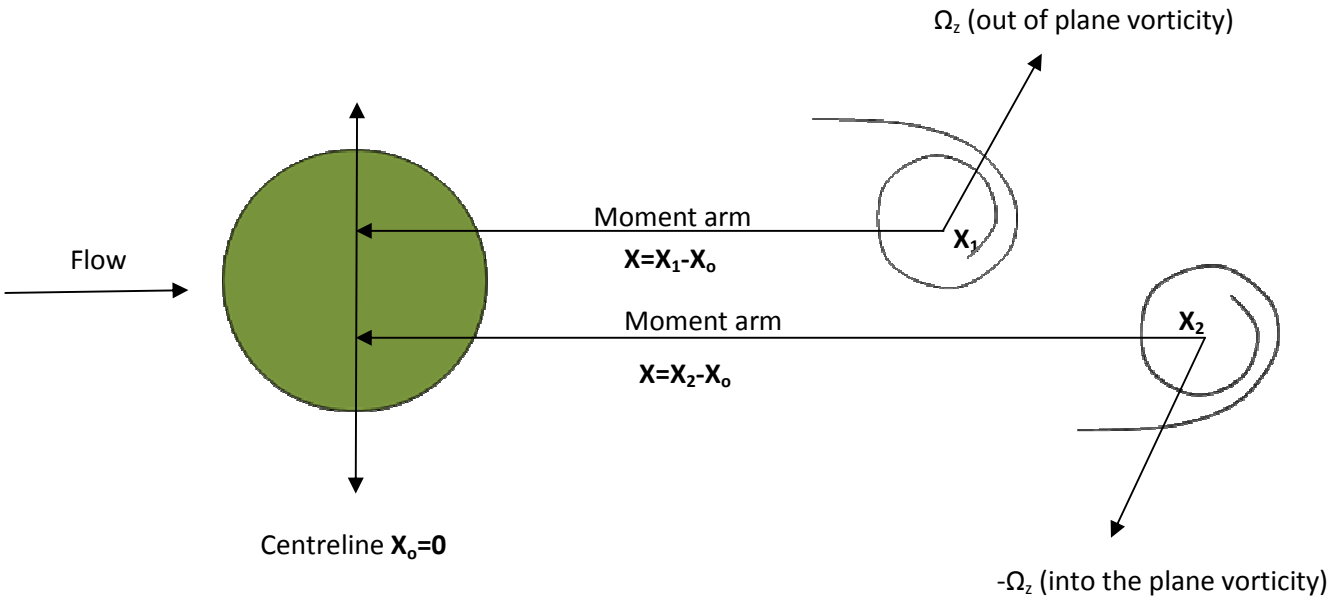

Figure 17: Schematic showing the problem set-up used in the lift estimation procedure

To arrive at the lift coefficients of the no slip and slip cylinders, 2-D PIV was done at the mid-section of the cylinders and the velocity vectors were computed. Figure 17 shows the problem set up used to estimate the lift coefficient. A control volume was

chosen extending from the beginning of the wake up to 5 cylinder diameters downstream. The velocity data was obtained as a grid of values, grid spacing depending on the interrogation window size and the overlap percentage chosen during PIV analysis. Vorticity was computed using a circulation estimate (Raffel, Willert, Wereley, & Kompenhans, 2007). The circulation method estimates the vorticity at point i, j using velocity values at the neighboring 8 points, using the stencil shown in Figure 18. The method calculates a circulation estimate for the whole area enclosed by the stencil. This was then divided by the area of the complete stencil to arrive at an average vorticity estimate for the whole stencil. This gave the vorticity at the point (i,j) of the stencil. The vorticity estimate at point (i,j) is given by:

$$(\omega_z)_{i,j} = \frac{\Gamma_{i,j}}{4\Delta X \Delta Y}. \tag{3.2}$$

Where, the circulation $\Gamma_{i,j}$ is given as:

$$\begin{aligned}\Gamma_{i,j} &= \frac{1}{2}\Delta X(U_{i-1,j-1} + 2U_{i,j-1} + U_{i+1,j-1}) \\ &+ \frac{1}{2}\Delta Y(V_{i+1,j-1} + 2V_{i+1,j} + V_{i+1,j+1}) \\ &- \frac{1}{2}\Delta X(U_{i+1,j+1} + 2U_{i,j+1} + U_{i-1,j+1}) \\ &- \frac{1}{2}\Delta Y(V_{i-1,j+1} + 2V_{i-1,j} + V_{i-1,j-1}).\end{aligned} \tag{3.3}$$

In the above formula, *U* and *V* are the X and Y velocities at the various grid points, and *δX* and *δY* are the grid spacing in the X and Y direction. The stencil was coded up and vorticity was estimated at each point. A time series of spatial vorticity fields was computed from the velocity data. An example of a vorticity snapshot is shown in Figure 19 for the no-slip cylinder and the spray painted superhydrophobic cylinder at a Reynolds Number of 4160. Figure 19, in addition to providing an example of the

contours obtained by the lift formulation, also provides a nice visual comparison between the vortex structure of the slip and the no slip cylinders. Vortices shed from the smooth cylinder were more coherent and interlaced with each other, while those shed from the slip cylinder were not as coherent and were interlaced less. The vortices from the slip case were also shed more parallelly as compared to the smooth case where the vortices form a rhythmic alternate pattern. Equation (1.3) was applied on the control volume and on the walls of the control surface to obtain the lift force as a function of time, shown in Figure 20. The RMS lift coefficients obtained using the above method gave an average lift coefficient for the no-slip case of $C_{L,RMS}=2.3\pm0.2$. This value is similar to what was observed by Noca (Noca, Shiels, & Jeon, 1997) and other 2-D measurements of lift from a cylinder. Figure 20 shows a comparison between the lift coefficient response of a no-slip cylinder and those of two superhydrophobic slip cylinders at a Reynolds Number of Re=4160. The first is a Teflon cylinder made superhydrophobic by sanding it with 320-grit sandpaper (Nilsson, Daniello, & Rothstein, 2010) and the second is a cylinder spray painted with a superhydrophobic paint (Cytonix LLC, WX2100^{TM}). From Figure 20, it is clear that the amplitude of oscillations is reduced by the superhydrophobic surface while the frequency is either unchanged (sanded Teflon cylinder) or is slightly reduced (spray painted cylinder). Lift coefficient obtained is not perfectly sinusoidal, but rather grows and shrinks. This observation is similar to those of Rockwell et al. (Lin & Rockwell, 1996) and Noca et al. (Noca, Shiels, & Jeon, 1997).

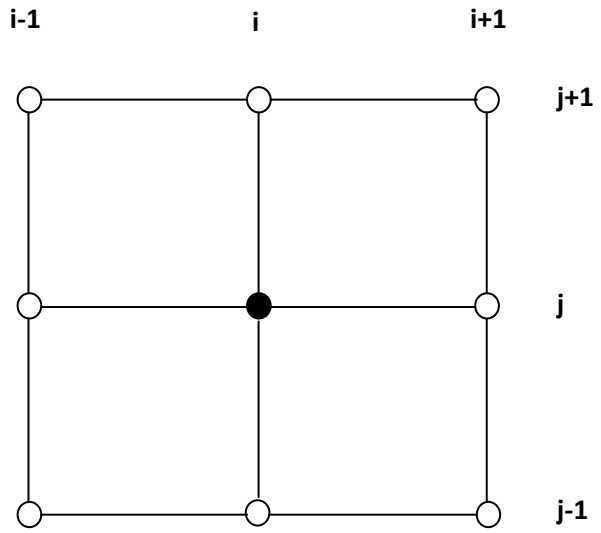

Figure 18: Schematic showing the stencil used in estimation of vorticity in the wake of the cylinders.

The lift coefficients obtained from the cylinders are non-dimensionalized relative to the no slip cylinder and the coefficients are presented on a scale of 0-1, one representing the lift coefficients of the no slip case. From Figure 21, it is evident that both the ridged and the random slip surfaces reduce the RMS lift coefficient of the cylinder by approximately 15-20 %.

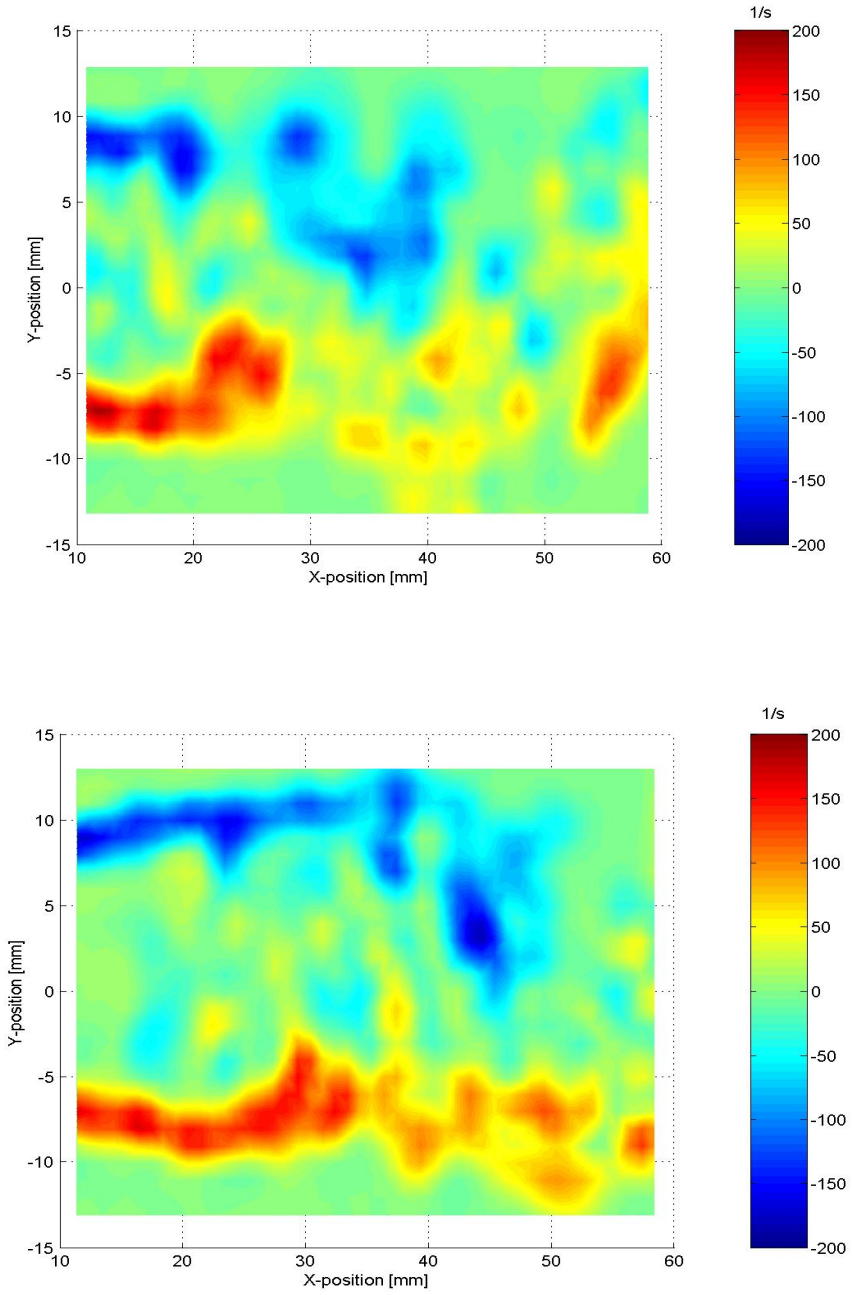

Figure 19: Vorticity contours obtained using the lift estimation procedure used in the current work, of the smooth cylinder (top) and a superhydrophobic spray painted cylinder (bottom) at Re=4166. Centers of the cylinders (not shown in figure) are at X=Y=0.

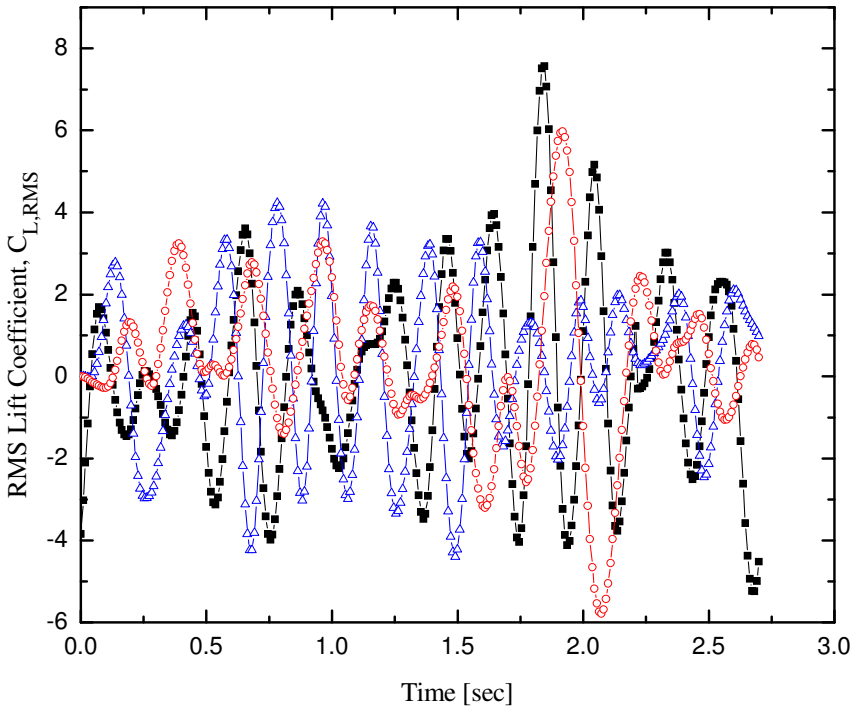

Figure 20: Time trace of RMS lift coefficient, $C_{L,RMS}$ for a smooth cylinder (■), a Teflon cylinder sanded with 320-grit sandpaper (8) and a cylinder painted with superhydrophobic paint (*O*), showing the reduction in the lift force as a result of slip

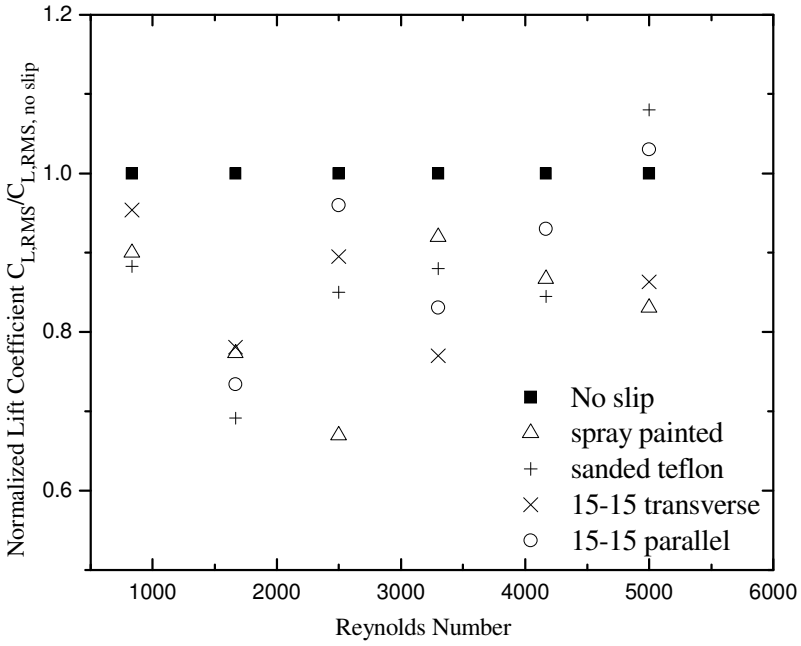

Figure 21: Normalized lift coefficient, $C_L/C_{L,\ no\text{-}slip}$, as a function of Reynolds Number showing that superhydrophobic cylinders produce less RMS lift compared to smooth cylinders. The data include: smooth cylinder (■), superhydrophobic cylinder produced using commercial superhydrophobic spray paint (8), a superhydrophobic cylinder produced by sanding a Teflon cylinder (□), a cylinder with *w*=15*μ*m wide microridge spaced *d*=15*μ*m apart aligned transverse to the flow (X) and a superhydrophobic cylinder with *w*=15*μ*m wide microridge spaced *d*=15*μ*m apart aligned parallel to the flow (*O*)

CHAPTER 4

CONCLUSIONS

Flow past bluff bodies is a phenomenon that has been studied quite well. This flow involves interesting phenomena like flow separation, vortex shedding and vibrations in the cross flow direction. However there has not been any experimental work dealing with the flow past bluff bodies with slip. This thesis is the first to probe that aspect of bluff body flow. In this work, cylinders with a coating of slip (superhydrophobic cylinders) were tested in a water tunnel and the dynamics of the flow past them were studied. The slip surfaces were either fabricated as ridges of slip or were random in nature. The directional slip surfaces were fabricated out of PDMS with a combination of soft- and photo-lithography and had ridges of slip on the surface, either transverse or parallel to the flow. The random slip surfaces were fabricated by either sanding Teflon cylinders with 320-grit sandpaper or by spray painting a smooth cylinder with a superhydrophobic paint. All the wake characteristics and the drag and lift of the ridged slip cylinders were studied while certain wake and shedding characteristics and the lift of the random slip case were studied and compared to the smooth case. It was found that slip delayed the onset of shedding. It also reduced the strouhal number in the case of the transverse ridges of slip and for the spray paint while it increased the strouhal number in the case of the parallel ridges of slip. For the sanded Teflon case, there was no change in the strouhal number. The slip cylinders shed vortices which were elongated in the flow direction, were less interlaced and were weaker than the vortices shed from the smooth case. It was also found that these surfaces had a considerable impact on the swirling strength, turbulent kinetic energy in the wake and the lift force acting on the cylinders.

However, no differences in drag could be identified. This could be due to the domination of the pressure drag over the friction drag for a bluff body. The results obtained in this work correspond to a Knudsen Number (ratio of slip length to cylinder radius) of the order of 0.01. Legendre et al. (Legendre, Lauga, & Magnaudet, 2009) show from their simulations that slip on a bluff body becomes more effective as the Knudsen number grows. Hence the effects that were seen in this thesis would be amplified in the case of microfluidic devices incorporating bluff body flows, since the Knudsen numbers in these devices would be of O(1). The experiments done in this thesis were in the regime of Reynolds Numbers where the boundary layer around the cylinder was still laminar. Provided the survivability of the surface, it would be interesting to see the effect of these surfaces in the turbulent regime where the boundary layer is very much thinner and approaches the order of the superhydrophobic feature size. The results from this study could also be related to flow past hydrofoils where both shear flow effects and separation flow effects compete.

BIBLIOGRAPHY

[1] Adrian, R. J., Christensen, K. T., & Liu, Z. C. (2000). Analysis and interpretation of instantaneous turbulent velocity fields. *Experiments in Fluids* , 275-290.

[2] Balasubramanian. (2010). Microstructured hydrophobic surfaces. *Journal of Fluid Mechanics* .

[3] Balasubramanian, A. K., Miller, A. C., & Rediniotis, O. K. (2004). Microstructured hydrophobic skin for hydrodynamic drag reduction. *AIAA J. 42* , 411-414.

[4] Barthlott, W., & Neinhuis, C. (1997). Purity of the sacred lotus, or escape from contamination in biological surfaces. *Planta* , 1-8.

[5] Beaudan, P., & Moin, P. (1994). Numerical experiments on the flow past a circular cylinder at sub-critical Reynolds number. Stanford: Stanford University.

[6] Benard, H. (1908). The formation of gyration centres at the back of a moving obstacle. *C. R. Acad. Sci.* , 839-842.

[7] Bhushan, B., & Jung, Y. C. (2006). Micro- and nanoscale characterization of hydrophobic and hydrophilic leaf surfaces. *Nanotech* , 2758-2772.

[8] Bico, J., Marzolin, C., & Quere, D. (1999). Pearl drops. *Europhys. Letters* , 220-226.

[9] Blackburn, H., & Melbourne, W. (1996). The effect of free-stream turbulence on sectional lift forces on a circular cylinder. *Journal of Fluid Mechanics* , 267–292.

[10] Brede, M., Eckelmann, H., & Rockwell, D. (1996). On secondary vortices in the cylinder wake. *Phys. Fluids* , 2117-2124.

[11] Cassie, A. B., & Baxter, S. (1944). Wettability of porous surfaces. *Trans. Faraday Soc.* , 546-551.

[12] Choi, C. H., & Kim, C. J. (2006). Large slip of aqueous liquid flow over a nanoengineered superhydrophobic surface. *Phys. Rev. Lett.* , 066001.

[13] Choi, C.-H., Ulmanella, U., K., J., Ho, C.-M., & Kim, C.-J. (2006). Effective slip and friction reduction in nanograted superhydrophobic microchannels. *Phys. Fluids* , 087105.

[14] Daniello, R. (n.d.). Personal Communication.

[15] Daniello, R., Waterhouse, N. E., & Rothstein, J. P. (2009). Turbulent drag reduction using superhydrophobic surfaces. *Phys. Fluids.* , 085103.

[16] Drescher, H. (1956). Messung der auf querangestr.omte Zylinder ausge.ubten zeitlich ver.anderten. *Dr.ucke. Zeitschrift f .ur Flugwissenschaften und Weltraumforschung* , 17–21.

[17] Fukagata, K. K. (2006). A theoretical prediction of friction drag reduction in turbulent flow by superhydrophobic surfaces. . *Phys. Fluids* , 051703.

[18] Gogte, S., Vorobieff, P., Truesdell, R., Mammoli, A., van Swol, F., Shah, P., et al. (2005). Effective slip on textured superhydrophobic surfaces. *Phys. Fluids* , 051701.

[19] Henoch, C., Krupenkin, T. N., Kolodner, P., Taylor, J. A., Hodes, M. S., Lyons, A. M., et al. (2006). Turbulent drag reduction using superhydrophobic surfaces. *AIAA Flow Control Conference.* San Francisco, CA.

[20] Joseph, P., Cottin-Bizonne, C., Benoit, J.-M., Ybert, C., Journet, C., Tabeling, P., et al. (2006). Slippage of water past superhydrophobic carbon nanotube forests in microchannels. *Phys. Rev. Lett.* , 156104.

[21] Kravchenko, A., & Moin, P. (1998). *B-spline methods and zonal grids for numerical simulations of turbulent flows.* Stanford: Flow Physics and Computational Division, Department of Mechanical Engineering, Stanford University.

[22] Lamb, S. (1945). *Hydrodynamics.* Dover Publications.

[23] Lauga, E., & Stone, H. A. (2003). Effective slip in pressure driven stokes flow. *J. Fluid Mech* , 55-77.

[24] Leal, L. G. (1992). Laminar flow and convective transport processes: Scaling principles and asymptotic analysis. Boston: Butterworth-Heinemann.

[25] Leal, L. G. (1989). Vorticity transport and wake structure for bluff bodies at finite reynolds number. . *Phys. Fluids* , 124-131.

[26] Lee, C., & Kim, C.-J. (2009). Maximizing the giant liquid slip on superhydrophobic microstructures by nanostructuring their sidewalls. *Langmuir* , 12812-12818.

[27] Legendre, D., Lauga, E., & Magnaudet, J. (2009). Influence of slip on the dynamics of two-dimensional wakes. . *J. Fluid Mech.* , 437-447.

[28] Lighthill, J. (1986). Fundamentals concerning wave loading on offshore structures. *J. Fluid Mech* , 667-681.

[29] Lim, H.-C., & Lee, S. J. (2002). Flow control of circular cylinders with longitudinal grooved surfaces. *AIAA J.* , 2027-2036.

[30] Lin, J. C., & Rockwell, D. (1996). Force identification by vorticity fields: Techniques based on flow imaging. *Journal of Fluids and Structures* , 663-668.

[31] MacDonald, M. J., & Muller, S. J. (1997). Shear rheology of polymer solutions near the critical condition for elastic instability. *Rheol. Acta* , 97-109.

[32] Magnaudet, J., & Mougin, G. (2007). Wake instability of a fixed spheroidal bubble. *J. Fluid Mech* . , 311-337.

[33] Martell, M. B., Perot, J. B., & Rothstein, J. P. (2009). Direct numerical simulations of turbulent flows over superhydrophobic surfaces. *J. Fluid Mech.* , 31-41.

[34] Martell, M. B., Rothstein, J. P., & Perot, J. B. (2010). An analysis of superhydrophobic turbulent drag reduction mechanisms using direct numerical simulation. *Phys. Fluids* , 065102.

[35] McHale, G., Shirtcliffe, N. J., Evans, C. R., & Newton, M. I. (2009). Terminal velocity and drag reduction measurements on superhydrophobic spheres. *App. Phys. Lett.* , 064104.

[36] Min, T., & Kim, J. (2004). Effects of hydrophobic surfaces on skin-friction drag. *Phys. Fluids* , L55-L58.

[37] Navier, C. L. (1823). Memoire sur les lois du mouvement des fluides. *Memoires de l'Academie Royal des Sciences de I'Institut de France* , 389-440.

[38] Nilsson, M. A., Daniello, R. J., & Rothstein, J. P. (2010). A novel and inexpensive technique for creating superhydrophobic surfaces using Teflon and sandpaper. *Journal of Physics D-Applied Physics* .

[39] Noca, F. (1997). On the evaluation of time dependent fluid-dynamic forces on bluff bodies. . Pasadena: California Institute of Technology.

[40] Noca, F., Shiels, D., & Jeon, D. (1997). Measuring instantaneous fluid dynamic forces on bodies, using only velocity fields and their derivatives. *Journal of Fluids and Structures* , 345-350.

[41] Norberg. (2003). Fluctuating lift on a circular cylinder: review and new measurements. *Journal of Fluids and Structures* , 57-96.

[42] Oner, D., & McCarthy, T. J. (2000). Ultrahydrophobic surfaces: Effects of topography length scales on wettability. *Langmuir* , 7777-7782.

[43] Ou, J., & Rothstein, J. P. (2005). Direct velocity measurements of the flow past drag-reducing ultrahydrophobic surfaces. *Phys. Fluids* , 103606.

[44] Ou, J., Perot, J. B., & Rothstein, J. P. (2004). Laminar drag reduction in microchannels using ultrahydrophobic surfaces. *Phys. Fluids* , 4635-4660.

[45] Pope, S. B. (2003). *Turbulent flows* . New York, NY: Cambridge University Press.

[46] Raffel, M., Willert, C., Wereley, S., & Kompenhans, J. (2007). *Particle Image Velocimetry: A practical guide, 2 ed.* Springer.

[47] Rothstein, J. P. (2010). Slip on superhydrophobic surfaces. *Annu. Rev. Fluid Mech.* , 89-109.

[48] Shi, L. L., Liu, Y. Z., & Wan, J. J. (2010). Influence of wall proximity on charactersistics of wake behind a square cylinder: PIV measurements and POD analysis. *Exp. Thermal and Fluid Sci.* , 28-36.

[49] Strouhal, V. (1878). Uber eine besondere art der tonerregung. . *Annalen der Physik und Chemie 5* , 216-251.

[50] Strouhal, V. (1878). Uber eine besondere art der tonerregung. *Annalen der Physik und Chemie* , 216-251.

[51] Truesdell, R., Mammoli, A., Vorobieff, P., van Swol, P., & Brinker, C. J. (2006). Drag reduction on a patterened superhydrophobic surface. *Phys. Rev. Lett.* , 044504.

[52] Von Karman, T. (1911). Uber den mechanismus den widerstands, den ein bewegter korper in einer flussigkeit erfahrt. *Gottingen Nachr. Math. Phys. Kl.* , 509-517.

[53] Watanabe, K., Udagawa, Y., & Udagawa, H. (1999). Drag reduction of newtonian fluid in a circular pipe with highly water-repellent wall. . *J. Fluid Mech.* , 225-238.

[54] Wenzel, R. N. (1936). Resistance of solid surfaces to wetting by water. *Ind. Eng. Chem.* , 988-994.

[55] West, G., & Apelt, C. (1993). Measurements of fluctuating pressures and forces on a circular cylinder in the Reynolds number range 10^4 to $2.5x10^5$. *Journal of Fluids and Structures* , 227–244.

[56] Williamson, C. H. (1996). Vortex dynamics in the cylinder wake. *Annu. Rev. Fluid Mech.* , 477-539.

[57] Xia, Y., & Whitesides, G. (1998). Soft lithography. *Annu. Rev. Mater. Sci.* , 153-84.

[58] Ybert, C., Barentin, C., Cottin-Bizonne, C., Joseph, P., & Bocquet, L. (2007). Achieving large slip with superhydrophobic surfaces: Scaling laws for generic geometries. *Physics of Fluids* , 123601.

[59] You, D., & Moin, P. (2007). Effects of hydrophobic surfaces on the drag and lift of a circular cylinder. *Phys. Fluids* , 081701.

[60] Zdravkovich, M. M. (1981). Review and classification of various aerodynamic and hydrodynamic means for suppressing vortex shedding. *J. Wind Eng. Ind. Aero.* , 145-189.

[61] Zhang, X., Shi, F., Niu, J., Jiang, Y., & Wang, Z. (2008). Superhydrophobic surfaces: From structural control to functional application. *J. Mater. Chem.* , 621-26.